



HAL
open science

Granitic inselberg erosion controlled by dike swarm array in semiarid Brazil

Anna S.V. Souza, Rubson Maia, Francisco Bezerra, Piotr Migoń, Lionel Siame

► To cite this version:

Anna S.V. Souza, Rubson Maia, Francisco Bezerra, Piotr Migoń, Lionel Siame. Granitic inselberg erosion controlled by dike swarm array in semiarid Brazil. *Geomorphology*, In press, 440, pp.108865. 10.1016/j.geomorph.2023.108865 . hal-04183537

HAL Id: hal-04183537

<https://hal.science/hal-04183537>

Submitted on 19 Aug 2023

HAL is a multi-disciplinary open access archive for the deposit and dissemination of scientific research documents, whether they are published or not. The documents may come from teaching and research institutions in France or abroad, or from public or private research centers.

L'archive ouverte pluridisciplinaire **HAL**, est destinée au dépôt et à la diffusion de documents scientifiques de niveau recherche, publiés ou non, émanant des établissements d'enseignement et de recherche français ou étrangers, des laboratoires publics ou privés.

1

2 **Granitic inselberg erosion controlled by dike swarm array**

3 **in semiarid Brazil**

4 Anna S. V. Souza*¹, Rubson P. Maia¹, Francisco H. Bezerra², Piotr Migoń³, Lionel L. Siame⁴

5

6 * Corresponding author

7 ¹ Department of Geography, Federal University of Ceará, Fortaleza, Brazil

8 ² Department of Geology, Federal University of Rio Grande do Norte, Natal, Brazil

9 ³ Institute of Geography and Regional Development, University of Wrocław, pl.

10 Uniwersytecki 1, 50-137 Wrocław, Poland

11 ⁴ Aix-Marseille Univ, CNRS, IRD, INRAE, CEREGE, Aix-en-Provence, France

12

13 **Abstract**

14 Numerous inselbergs rise above the regional erosional surface in semiarid northeastern
15 Brazil. The inselbergs are underlain by the Quixadá Pluton and cut by cm-thick granite dike
16 swarms. Five inselbergs with abundant dikes from two different parts of the pluton were
17 selected to investigate the role of dike patterns in the evolution of residual granite topography,
18 including morphological features of hillslopes. The methods included field mapping of
19 landforms, structural measurements of accessible dike arrays, and rock strength determinations
20 using a Schmidt hammer. Unmanned Aerial Vehicle (UAV) photogrammetry was used to build
21 detailed digital surface models of inselbergs and to recognize geometric patterns of dike arrays.
22 In addition, more than 30 rock samples were collected to determine rock composition and
23 evaluate their resistance to weathering. The results show that > 60% of dikes display a sub-
24 horizontal array composed of low- and medium-angle dikes (up to 45° dip), which tend to

25 increase rock-mass resistance, providing effective barriers against weathering and vertical
26 fracturing, and are associated with the most prominent, steep-sided residual hills. Besides, dike
27 swarm geometry controls the slope outlines of some inselbergs, which commonly conform to
28 dike attitudes. By contrast, steeply-dipping dikes ($> 60^\circ$ dip) promote weathering along the
29 dike-host rock interface and are hypothesized to underlie the plains between the inselbergs. At
30 a small scale, dikes control the occurrence and evolution of minor rock landforms such as
31 weathering pans, solution runnels, overhangs, and split boulders. Our findings show that the
32 resistance of inselbergs to erosion is not homogeneous in the granitic pluton but is controlled
33 by local factors such as dike occurrence and dip.

34 **Keywords:** Inselbergs; structural control; dikes; UAV

35 1. Introduction

36 Inselbergs are among the most characteristic landforms built of granite (Thomas, 1978;
37 Twidale, 1982; Twidale and Vidal-Romaní, 2005; Migoñ, 2006). This name, coined at the turn
38 of the 20th century and widely adopted afterward, applies to isolated hills rising above flat or
39 gently undulating denudation surfaces (the name itself is German and literally means ‘island
40 hill’). Many inselbergs show sharp slope/piedmont junctions and steep, not uncommonly bare
41 rock slopes along part of their perimeters. Inselbergs as medium-scale relief features typically
42 host smaller-scale landforms such as boulders, tafoni, weathering pits, rillenkarrren and non-
43 karstic caves developed along deep joint-controlled clefts or between boulders. Inselbergs have
44 been reported from various climatic settings (see reviews in Twidale, 1982 and Migoñ, 2006),
45 suggesting a minor role of climatic control and the primary role of rock properties in landform
46 evolution in granite areas.

47 Scientific debates about granite inselbergs have focused on two key, interrelated issues, with
48 two main questions: the origin of residual hills and the reasons for the emergence and survival
49 of a hill in a specific place. Regarding the former, the concept of two/multi-stage origin,
50 involving the phase of deep selective weathering, followed by removal of weathering products
51 and exposure of unweathered granite compartments, gained widespread acceptance (Thomas,
52 1965, 1978; Twidale, 2002) and empirical confirmation from observations in deep excavations,
53 drillings and geophysical surveys (Lidmar-Bergström, 1989; Beauvais et al., 2003). For very

54 high inselbergs, alternating phases of deep weathering and regolith erosion are more likely than
55 a simple replacement of weathering by erosion (Twidale and Bourne, 1975). This model applies
56 to humid environments, where deep weathering systems are particularly efficient, but inselbergs
57 in contemporary arid and semiarid areas may be inherited from previous, more humid climates.

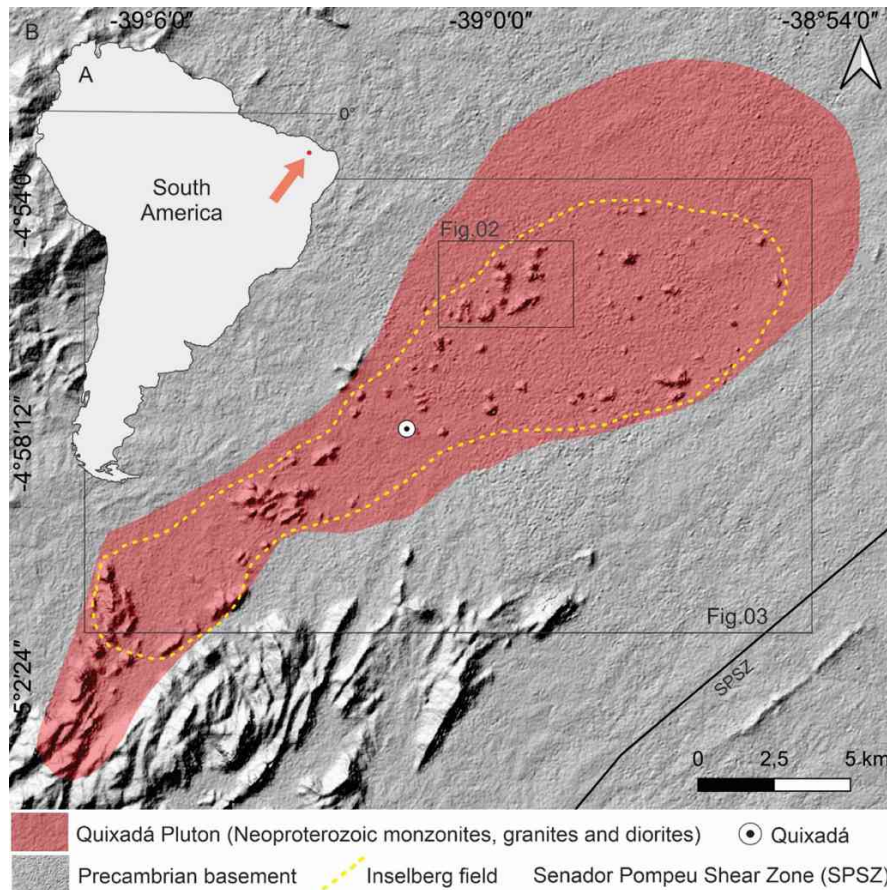
58 Reasons for the selectivity of deep weathering may be lithological or structural. Granite
59 plutons are not necessarily lithologically homogeneous, and potassium-rich granites tend to
60 give rise to inselbergs more readily than other variants (Pye et al., 1986; Migoñ, 1996).
61 Likewise, late-stage intrusions of finer-grained variants into coarse-grained granites from the
62 main intrusive phase are more resistant and support residual hills (Migoñ, 1996). However,
63 most granite inselbergs seem to be structure-controlled landforms (Twidale, 1982, 1998;
64 Römer, 2005, 2007; Migoñ, 2006), resulting from heterogeneous bedrock fracture densities,
65 which allow more massive compartments to resist weathering and remain in relief after
66 differential erosion (Thomas, 1965, 1978; Twidale, 1982; Twidale and Vidal-Romaní, 2020).
67 Many granite inselbergs, including various classic localities in Brazil (Lima and Corrêa-Gomes,
68 2015; Varajão and Alkmin, 2015), are massive hundreds of meters high domes with continuous
69 joint traces tens of meters apart. In fact, if structural control is so strong, the preparatory phase
70 of deep weathering is not essential, and inselbergs may reflect different joint-related efficacies
71 of surface weathering systems, as demonstrated for impressive granite inselbergs of the Namib
72 Desert (Selby, 1982).

73 The structural aspect also comprises elements such as systems of veins and dikes (Migoñ,
74 2004), which are frequent in igneous bodies and widely studied from a geological point of view
75 (Halls, 1982; Ernst and Buchan, 2006; Gonnermann and Taisne, 2015; Fossen, 2016). In
76 contrast, they have received relatively scarce attention in geomorphological research. Studies
77 carried out by Johnson (1968), André (2002), Jürgens and Burke (2000) and Nicholson (2008)
78 provided some insights into the issue of dike control. However, they did not address the role of
79 dikes/veins as the main theme, and certainly not in the context of the evolution of granite
80 inselbergs.

81 In semiarid Northeastern Brazil, many inselbergs and associated minor landforms occur
82 within intrusions of granitic composition (Vauchez et al., 1995; Maia and Nascimento, 2018;
83 Maia and Bezerra, 2020; Aragão et al., 2020). Among them is the Quixadá Pluton, located in
84 the central part of Ceará State, distinguished by the abundance of inselbergs (Maia et al., 2015).

85 Granites exposed within inselbergs are intensely cross-cut by felsic dike swarms (Almeida,
 86 1995; Nogueira, 2004). A few studies reported differential weathering processes related to dike
 87 and veins (Maia et al., 2015; 2022). However, no discussion has been presented regarding their
 88 significance for the broader-scale geomorphology of inselbergs.

89 To fill this gap, we use a combination of methods and aim: (i) to analyze the regional
 90 structural framework of Quixadá Pluton; (ii) to provide detailed characteristics of dike patterns
 91 in terms of composition, strength, and geometry; (iii) to verify how felsic dikes may guide
 92 differential weathering processes based on their compositional and geometric aspects, and
 93 therefrom (iv) to ascertain implications of the arrangement of felsic dike swarms on landform
 94 evolution in the Quixadá inselberg field. Therefore, this work intends to contribute to
 95 understanding inselberg evolution based on the perspective of structural geomorphology.



97 Fig. 1. Location map of Quixadá Pluton in NE Brazil, where the inselberg field is located (yellow dashed
 98 line). The Precambrian basement hosts the pluton; one of the major regional structures (SPSZ) is
 99 indicated in the southeast. Geological data based on Pinéo et al. (2020).

100 2. Location of the study area and geological setting of inselbergs

101 *2.1. Location and geological setting*

102 In Northeastern Brazil, an outstanding inselberg landscape is located around the town of
103 Quixadá, 170 km away from the Atlantic Ocean (Fig. 1). More than 60 inselbergs occur in
104 isolation or small clusters and rise from 30 m to 300 m high above the regional erosion surface
105 at approximately 150 m a.s.l., named the Sertaneja Surface (Costa et al., 2020) (Fig. 2). In the
106 south, the granite pluton borders with metamorphic massifs elevated to ca. 700 m a.s.l (Maia et
107 al., 2015; Costa et al., 2020). The climate of the area is semiarid (Alvares et al., 2013), with a
108 mean annual rainfall of 700 mm (Funceme, 2022) and a rainy season coinciding with summer-
109 autumn. The average temperatures are around 26 °C to 28 °C (INMET, 2022).

110 The Quixadá inselberg field is located at the center of a Precambrian block. The area is part
111 of the Borborema Province, formed during the Neoproterozoic Brasiliano Cycle, the last
112 orogeny in intraplate South America (640-540 Ma) due to the collision of Amazonas, São
113 Luis/West African and São Francisco/Congo cratons (Almeida et al., 2000). The Brasiliano
114 Cycle involved the origin of NE-SW-striking ductile strike-slip shear zones that accommodated
115 the intrusion of several igneous bodies (Vauchez et al., 1995). The region has been subjected to
116 brittle deformation until the present (Bezerra et al., 2011; Costa et al., 2020b).



118 Fig. 2. Quixadá inselberg field, in semiarid Brazil. The hills are supported by the Quixadá Pluton granitic
119 rocks and reach up to 430 m a.s.l, displaying a variety of morphologies. Location in Fig.1.

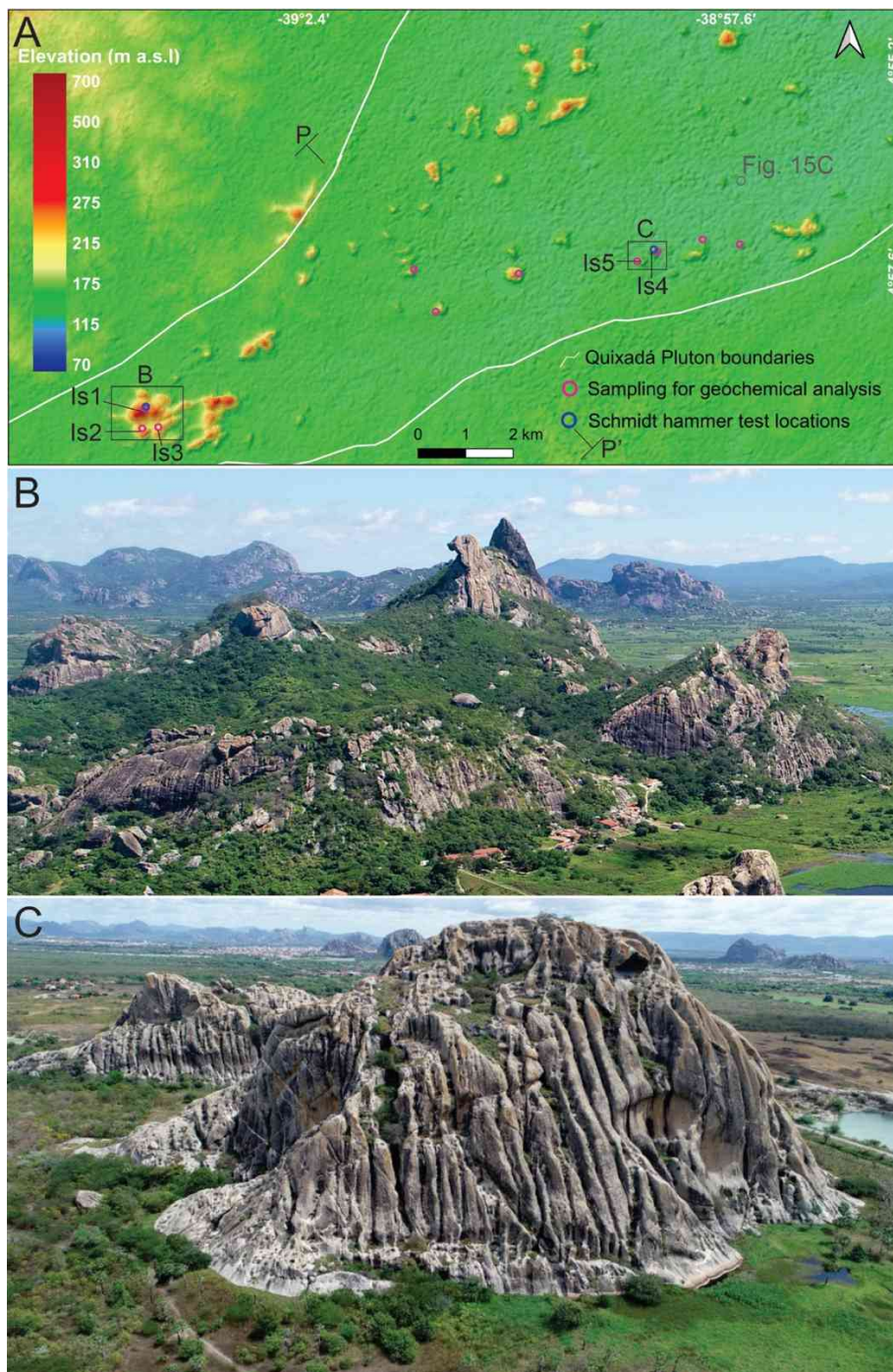
120 The Quixadá Pluton (ca. 31 x 8 km) (Fig. 1) is one of the Neoproterozoic granites that
121 intruded the Precambrian basement rocks, namely the Juatama Unit and Independência
122 Formation, situated in the Ceará Central Domain (Pinéo et al., 2020). The Quixadá Pluton
123 encompasses lithologies of the Itaporanga Intrusive Suite (600-585 Ma) of potassium-rich, calc-
124 alkaline affinity, composed of monzonites, quartz-monzonites, monzodiorites, and
125 granodiorites of porphyritic texture with potassium feldspar megacrysts immersed in a
126 phaneritic matrix (Mariano and Sial, 1990; Galindo et al., 2019; Pinéo et al., 2020). The
127 porphyritic monzonites constitute the main granitic facies, named the Quixadá Facies (Almeida,
128 1995; Pinéo et al., 2020), in which ellipsoidal mafic enclaves of dioritic composition are
129 enclosed (Almeida, 1995; Nogueira, 2004). Apart from the main igneous body, leuco-
130 microgranites and fine- to medium-grained equigranular granites *sensu stricto* occur as dikes
131 and veins (Galindo et al., 2019; Archanjo et al., 2002). These felsic dikes intruded porphyritic
132 rocks of the Quixadá Pluton and are referred to as felsic equigranular facies due to their high
133 silica content compared to the host rocks (Silva, 1989). They are syn-plutonic structures and
134 display geometric variations resulting from crystallization/melt fraction and consequent
135 fracturing (Almeida, 1995; Nogueira and Morales, 1999).

136 The Senador Pompeu Shear Zone is one of the most important regional structures close to
137 the pluton (Castro et al., 2002). This shear zone, along with other shear zones in the region,
138 guided pluton emplacement and local magmatic flow structures, such as crystal stretching and
139 elongation of mafic enclaves (Maia and Bezerra, 2020).

140 2.2. Inselbergs

141 The granitic facies of the Quixadá Pluton underlie the inselberg field. The inselbergs display
142 a variety of shapes. Maia et al. (2015) summarized morphological patterns in the Quixadá
143 inselberg field with regard to the weathering-related features, distinguishing three dominant
144 geomorphic types: (1) inselbergs with the rock mass densely fractured, modeled by frequent
145 rock-slope failures and surrounded by talus deposits, (2) inselbergs, whose bare slopes are
146 dominated by dissolution features, with limited evidence of rockfall, and (3) bornhardt-like
147 (domed) inselbergs with massive concave-convex slopes, very scarce evidence of rock fall and
148 almost no talus.

149 Among many inselbergs in the area, five were selected to conduct detailed studies of
150 hillslope morphology, weathering features and dike patterns (Fig. 3). These are coded IS1 to



151
 152 Fig. 3. Location and inselberg landforms in the study area (Quixadá, NE Brazil). The purple dots indicate
 153 sampling spots for geochemical analysis, and the blue dots indicate locations of outcrops where Schmidt
 154 hammer tests were performed. Profile P-P' is represented in Fig.6. A – Digital Surface Model of the
 155 Quixadá Inselberg Field. B – Oblique view of the inselberg cluster in the SW part of the pluton
 156 (inselbergs coded as IS1, IS2 and IS3). C – Oblique view of inselbergs in the E part of the pluton (IS4
 157 and IS5). Geological data based on Pinéo et al. (2020).

158
 159

160 IS5 and located in the southwestern (IS1, IS2, IS3) and the eastern part of the pluton (IS4, IS5).

161 Their morphology is summarized as follows:

- 162 • IS1 is one of the highest hills within the Quixadá Pluton, ca. 250 m high, with the
163 surrounding low-relief surface at approximately 200 m a.s.l. It has two sharply pointed
164 peaks with nearly vertical walls, aligned NE-SW and separated by a lower central sector
165 of convex shape, some 30 m below the level of the peaks. Extensive talus slopes meet
166 the adjacent plain at a ca. 20° angle and are built of metric and decametric boulders
167 derived from both upslopes and through in situ breakdown.
- 168 • IS2 is located south of IS1 and rises 120 m high. It is asymmetrical, with massive steep
169 east- and south-facing slopes and a gentle western slope. A few boulders are scattered
170 on the summit and occur in some adjacent sectors at the footslope. A large tafone, ~ 10
171 m long, occurs within the north-facing hillslope.
- 172 • IS3 is located east of IS2 and is 100 m high. The hillslopes are convex in the southern
173 and southwestern parts. In the central zone, slightly concave ramps occur, with scattered
174 decametric boulders. On the NE summit of the inselberg, a cave ca. 20 m long and 5 m
175 high has developed in porphyritic granite.
- 176 • IS4 is 110 m high and displays steep convex slopes, within which up to 80 m-long
177 parallel solution runnels have developed. However, no comparable features occur in the
178 massive granite exposed within the N/NW-facing slope.
- 179 • IS5 is located west of IS4 and ca. 65 m high. Only the east-facing slope is steep.
180 Otherwise, the hillsides gently slope toward the adjacent plain. In its northern sector,
181 decametric rock boulders (up to 19 m x 24 m) occur due to bedrock fragmentation.

182 3. Data sources, methods and terminology

183 This work is based on geomorphological, structural and petrological data derived from
184 satellite imagery, drone surveys, field mapping, testing of rock properties, and geochemical
185 analysis. Five inselbergs within the Quixadá Pluton were selected as sampling places (see
186 section 2.2), but the geomorphology of their surrounding areas was also considered.

187

188

189

190 3.1. Remote sensing survey

191 We performed a regional-scale analysis based on 12.5 m resolution ALOS PALSAR RTC
192 (AP_09568_FBS_F7080_RT1 and AP_2762_FBS_F7080_RT1 scenes), available on the
193 Alaska Satellite Facility platform (<https://asf.alaska.edu/>). These images allowed the
194 identification of major structures (e.g., shear zones) and geomorphological characteristics of
195 the area.

196 For detailed mapping, Unmanned Aerial Vehicle (UAV) surveys were carried out on five
197 inselbergs using DJI Phantom 4 Pro equipped with a 4K camera. The aerial images were
198 acquired by autonomous and manual mode flights at 100 m high (nadir viewing), with image
199 overlapping of 70%; photographs at 0° and 45° were taken at 30 m and 70 m of flight height,
200 respectively. Three flights were performed, the first covering an area of 1000 m x 1000 m
201 corresponding to IS1, the second covering an area of 500 m x 2000 m encompassing IS2 and
202 IS3, and the third flight covered an area of 800 m x 700 m encompassing IS4 and IS5. The
203 processing of aerial images provided georeferenced spatial datasets, including point clouds,
204 from which were derived 3D meshes, orthorectified photographs, and Digital Surface Models.
205 These products were elaborated in the Agisoft MetaShape software by the Structure from
206 Motion (SfM) algorithm, by which 2D aerial photographs are computed to reconstruct 3D
207 geometry of a scene, in our case, of inselbergs, based on parallax (Vollger and Cruden, 2016).

208 The UAV photogrammetry delivered an average spatial resolution of 20 cm for each point
209 cloud, and an orthophoto of 2-cm resolution. The high-resolution data allowed us to analyze
210 the topography of individual inselbergs and identify structural elements such as dikes, proving
211 to be a significant advance in local-scale geomorphological analysis, in relation to the
212 decametric-resolution of the regional-scale imagery, which does not allow for the identification
213 of the centimeter to 1-meter-thick features, for example.

214 3.1.1 Dike outcrop mapping

215 High-resolution orthophotographs and DSMs were exported to GIS program, and dike
216 outcrops were identified and mapped on each inselberg using QGIS software (3.16 version)
217 based on the nadir visualization. The line traces correspond to the areas where cm-thick dikes
218 intersect the surface/slope of the inselbergs as edges of planar bodies. Thus, the dike trace

219 identification depends more on the slope configuration rather than the geometry of the body. A
220 dike trace usually corresponds to dike segments visible in the present-day slope.

221 Thus, mapping the dike outcrops intends to show the visible configuration of how
222 centimeter-to-meter-thick dikes appear on inselbergs slopes. Therefore, these lineaments were
223 not considered to generate rose diagrams, as they do not reveal the strike of planar bodies.

224 *3.1.2 Extraction of dike attitudes*

225 Structural data of dike orientations was extracted using CloudCompare software (cloud
226 editing program). The dip and dip direction of the dikes were measured on dense point clouds
227 using the Virtual Compass/Plane Tool. The extraction of dike attitudes consists in fitting a plane
228 on an area of the point cloud where a dike plane is identified (the white color of leucogranite
229 dikes favored the identification of planar areas). The least square method is the statistical
230 method whereby the program provides the orientation value of a group of points (see further
231 details on Vollger and Cruden, 2016).

232 For each inselberg, 4 to 8 dike planes were selected to extract dike attitudes on point clouds.
233 The number of measurements is limited to the plane outcrops available for measurements,
234 which are only visible in parts of the rock mass where the host rock has been eroded. In each
235 selected dike plane, three measurements are extracted, and if consistency in dike attitude is
236 present (e.g., small variations in the angle of dip – up to 3°), the average value of attitude is
237 computed. This consistency allows us to confirm that the plane-fitting is on a dike plane and
238 not other parts of the slope.

239 These data sets and dike attitudes measured in the field were plotted in equal-area
240 stereographic projections. A total of 6 to 10 measurements of dike attitudes for each inselberg
241 was collected. Based on the analysis of these data, we also proposed a classification of the dike
242 array according to the dip angle range.

243 *3.2. Fieldwork*

244 Fieldwork involved landform inventory and mapping, especially with respect to the
245 manifestations of the dikes in hillslope morphology. Other features of interest included the
246 shapes of hillslopes and their changes, the occurrence and possible origin of boulders, caves
247 and rock shelters, and dissolution features (pans, karren, solution runnels). Wherever possible,
248 a representative amount of strike/dip data on individual dikes was measured with a Brunton

249 compass. Likewise, the thickness of dikes was measured in the field at accessible places. The
250 ductile (foliation) deformation pattern was assessed by visual analysis of change in foliation
251 and rock fabric within and outside the pluton, along with strike measurement of mineral
252 lineation.

253 Non-destructive Schmidt hammer tests were executed on rock outcrops to evaluate Uniaxial
254 compressive strength (UCS). The equipment used was an L-type Schmidt Hammer calibrated
255 in MPa reading units (measuring up to 100 Mpa). Fourteen rock outcrops were selected on
256 inselbergs IS1 and IS4, representing both dikes (8) and the host rock (6), and the following
257 procedure was adopted (Aydin, 2009). Twenty readings were taken on visibly non-weathered
258 rock surfaces, and the ten highest values were subject to further statistical analysis.

259 *3.3. Petrographic and geochemical analysis*

260 Thirty-four rock samples of dikes (20), host rock (11), and mafic enclaves (3) were collected
261 on outcrops (locations of sampling spots in Fig. 3). The samples were initially categorized by
262 the macroscopic petrographic aspects of the hand specimens (color, texture, and fabric), based
263 on Jerram and Petford (2011) descriptions (see sample photographs in Supplementary Material
264 A). The samples were ground at 200 – mesh on AMP1-M (AMEF Commercial Ltda) pan mill
265 equipment for geochemical analysis and submitted to Energy Dispersive X-Ray Spectroscopy
266 analysis in a desktop Scanning Electron Microscope (SEM_EDS TM3000). The results
267 provided the composition (%) of oxides in each sample: SiO₂; Al₂O₃; Na₂O; K₂O; FeO_t; MgO;
268 P₂O (see Supplementary Material B). The results of previous analyses of granite rocks from the
269 Quixadá Pluton (Silva, 1989; Almeida, 1995) were considered in the typology of dikes (see
270 section 4.1).

271 *3.4. Terminological remarks*

272 In this study, dikes are considered sheet-like tabular bodies of igneous rocks intruded into
273 preexisting bedrock in the late stages of magmatic activity, ranging from a few centimeters to
274 a few meters in thickness. They typically occur in swarms, consisting of a set of coeval
275 intrusions. Veins, in turn, are referred to as mineral-filled intrusions. These definitions are based
276 on Ernst and Buchan (2004), Gill (2010), Goonerman and Taisne (2015), and Korteniemi
277 (2015). Table 1 defines a few specific terms often used in this work.

278

279 **Table 1. Definitions of specific terms related to dike occurrence and applied in this study**

Term	Definition
Intersection point/line	The junction of the dike with the inselberg slope, which allows for the identification of a dike outcrop
Dike outcrop	The exposed surface of a dike, where its thickness can be measured
Dike – host rock interface	The contact between the border of the dike and its host rock
Dike intersection	Cross-cutting relationship between dikes
Dike orientation	Strike and dip of a dike
Dike array	The general geometrical mode of dike organization, according to the orientation and geometry of intrusions (e.g., vertical array, sub-horizontal array)

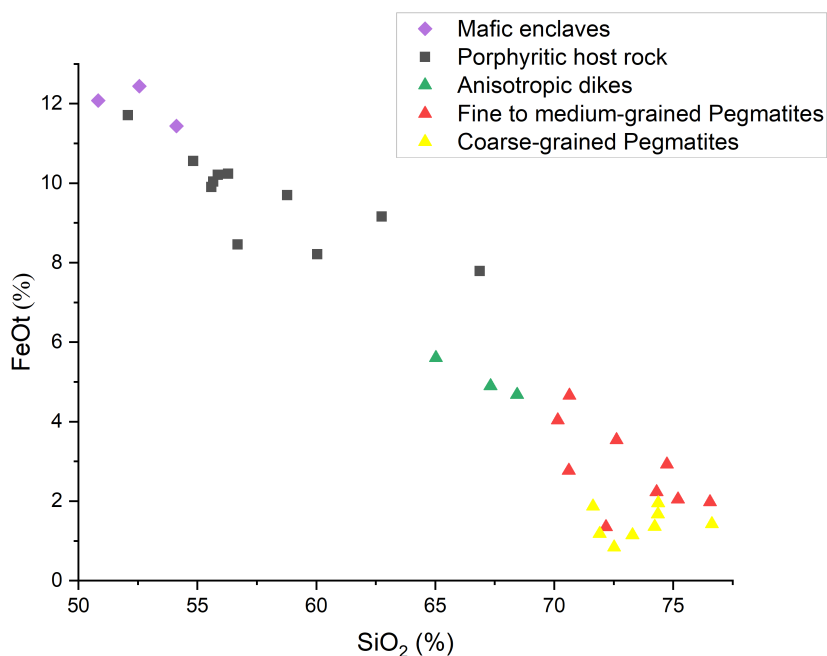
280 **4. Results**281 *4.1. Rock properties*282 *4.1.1 Compositional and textural aspects of the granite rocks*

283 The sheet intrusions within the Quixadá Pluton are generally of granite composition. They
 284 were distinguished into three types based on their macroscopic texture and fabric: fine-grained
 285 pegmatites, coarse-grained pegmatites, and anisotropic dikes.

286 Pegmatite dikes are the most common type of intrusion in the pluton and consist of
 287 centimeter-thick sheet-like bodies. They are leucocratic phaneritic and isotropic rocks, which
 288 display textural diversity reflecting the crystallization period. Thus, a few samples represent
 289 equigranular rocks of fine- or medium-grained texture (FgP), whereas others are non-
 290 equigranular and coarse-grained (CgP). In the latter, quartz and feldspar crystals are well-
 291 developed and distinguished from the mafic ones, such as biotite, which are nearly absent in
 292 some samples.

293 Anisotropic dikes (AD) are also phaneritic, with a fine- to medium-grained texture. They
 294 differ from pegmatites by their subtle anisotropy generated by mineral stretching and because
 295 they occur as meter-thick sheet intrusions. The color of the samples also allows for the
 296 identification, as they present a superficial grey color due to higher concentrations of mafic
 297 minerals in comparison with other dikes, reflected in their geochemistry.

298 The felsic dikes of the Quixadá Pluton are hosted by a rock of porphyritic texture, with K-
 299 feldspar megacrysts immersed in a medium to the coarse-grained matrix. These rocks host
 300 ellipsoidal mafic enclaves of microgranular texture (Almeida, 1995).



301

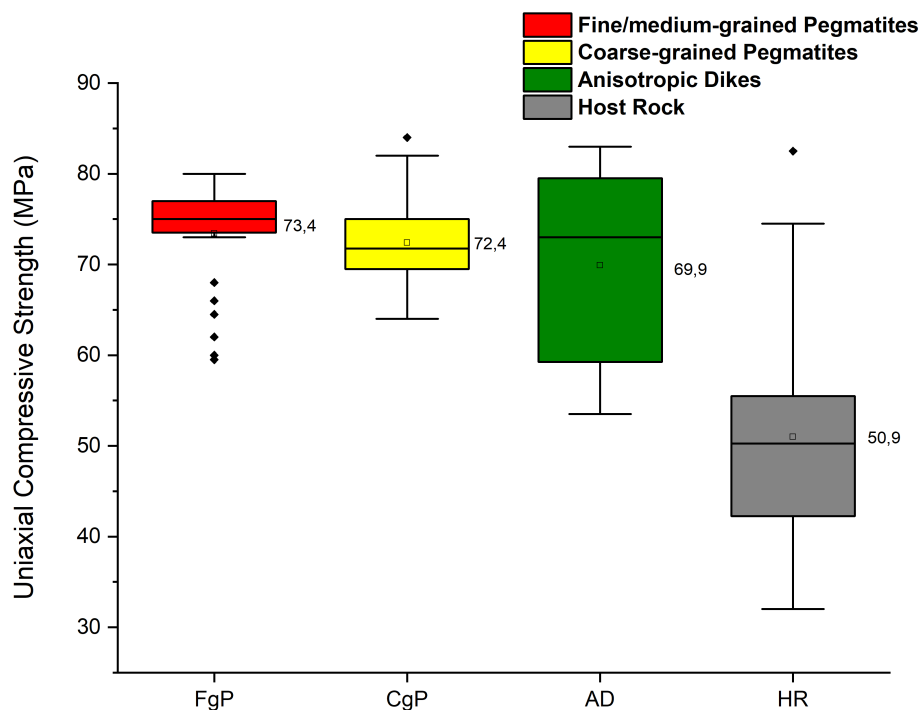
302 Fig. 4. FeOt x SiO₂ scatter diagram showing geochemical trends of more mafic/intermediate (left) and
 303 felsic (right) rock samples of the Quixadá Pluton. The location of the samples analyzed is indicated in
 304 Figure 3A.

305 The geochemical data (oxides %) from SEM/EDS analysis are provided in Supplementary
 306 Material B. In summary, samples of the host rock have an intermediate character (57% SiO₂
 307 avg.) and exhibit high FeOt (9.6% avg.) and MgO (4.9% avg.) contents. Dikes are generally
 308 richer in silica than the host rock, and the pegmatites (FgP and CgP) have higher silica content
 309 (73% avg) than the anisotropic dikes (66% SiO₂ avg.). The latter also have the highest
 310 proportion of elements indicative of mafic minerals among the felsic intrusions (5% FeOt avg.).
 311 The contrast between more acid and intermediate/basic granitic facies of the Quixadá Pluton
 312 rocks is illustrated by the FeOt versus SiO₂ plot (Fig. 4).

313 4.1.2. Geomechanical behavior

314 The Schmidt hammer tests indicate that the average Uniaxial Compressive Strength (UCS)
 315 slightly decreases from dikes to the host rock (Fig. 5). Despite the lack of visible signs of
 316 alteration, all rock surfaces are likely to be slightly affected by weathering once exposed to

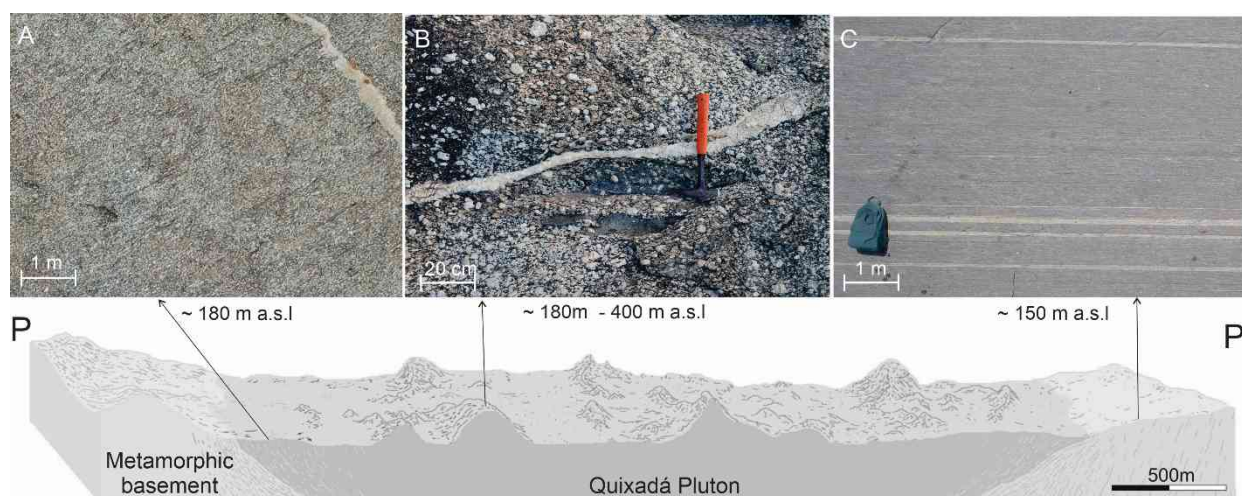
317 atmospheric agents, which affects rock strength. Therefore, the results do not exactly
 318 correspond to the mechanical behavior of fresh rocks.



319

320 Fig. 5. Box plot of UCS data on dikes (FgP – fine to medium-grained pegmatites; CgP – coarse-grained
 321 pegmatites; AD – anisotropic dikes) and host rock (HR). The values next to the boxplots are the mean
 322 UCS values for the granitic facies. The locations of the outcrops where Schmidt hammer tests were
 323 performed are indicated in Figure 3A.

324 The average UCS in all dikes is ca. 70 Mpa. The pegmatites yielded the highest surface
 325 strengths among the granitic facies. In more detail, rock strength of FgP varies between 60 Mpa
 326 and 80 Mpa, in a range similar to CgP, which presents a slightly higher maximum UCS value
 327 (84 Mpa). The strength values of AD, in turn, show a larger amplitude, with a minimum of 53
 328 Mpa and a maximum of 83 Mpa (for detailed data, see Supplementary Material C). The host
 329 rock displays the largest UCS range due to the evident differential strength of a porphyritic
 330 fabric, in which low UCS values (around 50 Mpa) are mainly related to the mafic matrix. In
 331 this portion of the rock, the impact of the Schmidt hammer plunger caused cracking of some
 332 minerals on the surface of the rock. In contrast, higher UCS values were recorded on potassium
 333 feldspar megacryst surfaces (usually about 70 Mpa). Small variations in surface hardness are
 334 related to texture contrasts.



335

336 Fig. 6. Schematic topographic profile illustrating the relation between geomorphological setting and
 337 change in foliation pattern in the Quixadá Pluton and its surroundings. The photographs show
 338 representative outcrops of each area. A – rock fabric with strong mineral foliation NE-striking. These
 339 rocks are located in the boundaries of the granitic pluton and underlie low outcrops at approx. 180 m
 340 a.s.l. B – typical outcrop of the Quixadá Pluton. Note that the rock is mostly isotropic with weak
 341 foliation in places marked by stretching of mafic enclaves. A granite dike cuts across the porphyritic
 342 rock. This lithology supports the landforms within the pluton, from 180 m to 400 m a.s.l. C – basement
 343 rocks with mylonite fabric, underlying low-relief areas outside the pluton of about 150 m a.s.l. Location
 344 in Fig.3 (profile P – P').

345 4.2 Structural aspects of the Quixadá Pluton – foliation and dikes

346 4.2.1. Regional foliation pattern and its relationship to topography

347 The porphyritic rocks of the Quixadá Pluton are mostly isotropic, displaying an occasional
 348 weak primary foliation marked by SW-NE stretching of some crystals (Fig. 6B) and orientation
 349 of some mafic enclaves. These rocks constitute the main facies encompassing the inselberg
 350 area, where, at the scale of analysis, no marked heterogeneities in the rock fabric were observed.
 351 Therefore, inselbergs are located randomly around their pluton, and no control of the foliation
 352 on the topography of the pluton was observed.

353 In contrast, an anisotropic fabric is exhibited by the rocks in the boundaries of the pluton,
 354 with a low-angle foliation and lineation (note the change in the fabric in Fig. 6A). These
 355 strongly foliated rocks do not support high relief. Thus, the overall topography of the pluton
 356 margins (east, west, and northern portions) is predominantly one of a plain, with low outcrops.

357 In the basement rocks, a mylonite fabric was identified (Fig. 6C) in outcrops located ca. 3
 358 km from the Senador Pompeu shear zone area, in the eastern portion outside the pluton (see

359 Fig.1 for the location of the SPSZ). The mylonites also underlie plain areas. Generally, a
 360 positive correlation between the degree of ductile deformation, expressed by foliation, and low-
 361 relief topography was noticed (see profile in Fig. 6).

362 4.2.2. Geometry and arrays of felsic dike swarms

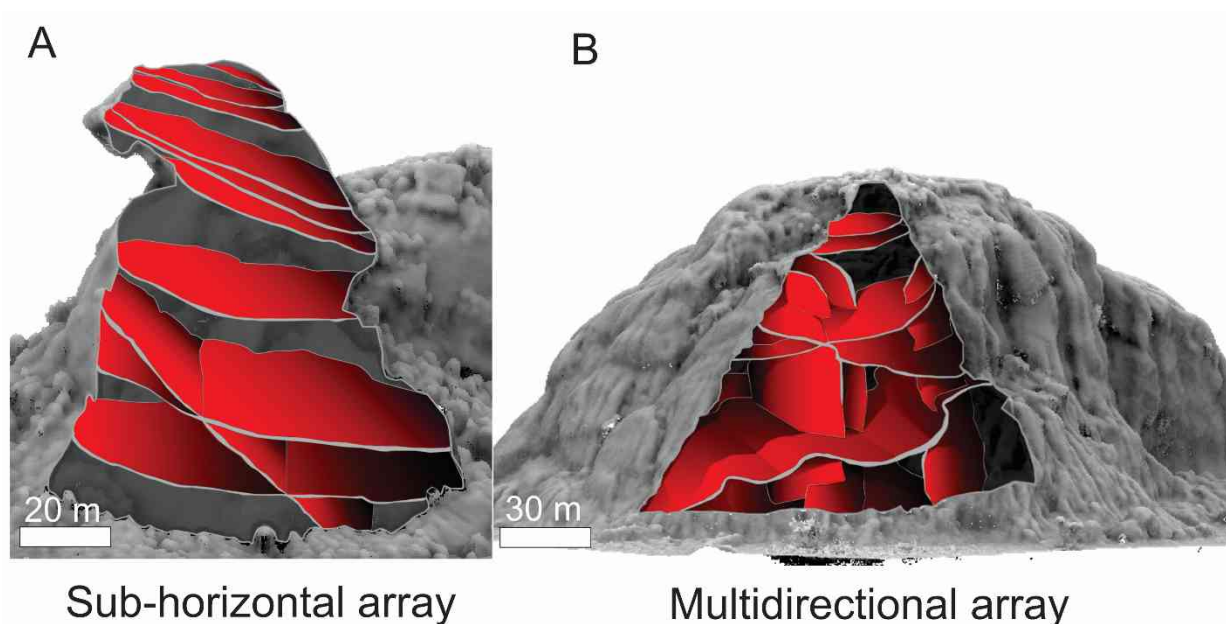
363 Granitic pegmatite dikes (FgP and CgP varieties) cut across porphyritic monzonites in the
 364 Quixadá Pluton. They are generally exposed on inselberg slopes as centimeter-thick intrusions
 365 (from 4 to 80 cm), with a few thicker intrusions reaching 1 m. The pegmatites display various
 366 strikes, and no direct correlation was observed with anisotropy in the host rock. Around the
 367 pluton area, the dike swarms are irregularly distributed. Field observations show more frequent
 368 occurrences (or better outcrops) of dikes in the southwestern and eastern sectors than in the
 369 north of the pluton, where few dike intrusions occur.

370 The dike swarms generally present a wide dip angle range, including individual dikes
 371 dipping from 1° to 77° (strike/dip data of individual dikes on each inselberg are provided in
 372 Supplementary Material E). Consequently, the dike pattern is classified according to the dip
 373 angle range for dike sets analyzed in each inselberg (Table 2).

374 **Table 2. Classification of dike pattern according to dip angle**

Dike pattern	Sub-horizontal dike pattern		Sub-vertical dike pattern	
Dip classification	Low-angle dikes	Medium-angle dikes	High-angle dikes	Very high-angle dikes
Range of dip angle	< 30°	31–45°	46–60°	> 60°

375
 376 Most dikes measured (62.5%) dip at low to moderate angles and thus form sub-horizontal
 377 arrays. In other cases, dike swarms display multidirectional arrays, including low-angle to high-
 378 angle dikes, in addition to bodies without a defined dipping plane, which display undulating
 379 shapes (deformed geometry) and/or gradational borders. Cross-cutting relationships between
 380 dikes are more frequent in this case than in arrays with more consistent attitudes. Figure 7
 381 illustrates these contrasting array patterns commonly found on the inselbergs of Quixadá.



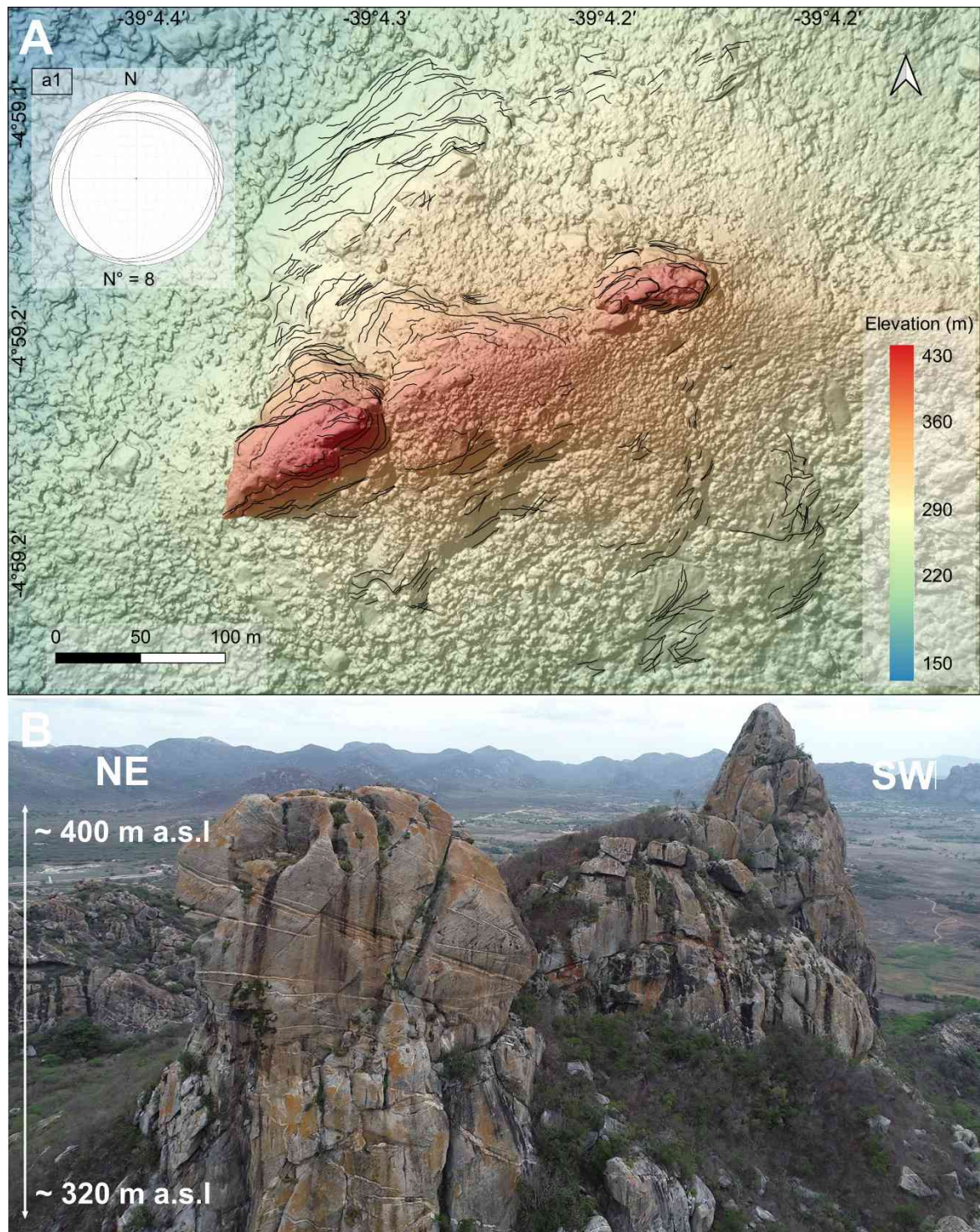
382

383 Fig 7. Models of dike arrays illustrating dike planes and their trending attitudes on inselbergs. A – Sub-
 384 horizontal dike array, with inclined dikes at low-angle and few intersections (Location in Fig. 3 – IS1).
 385 B – Multidirectional array composed of low- to high-angle dikes and dikes with more varied geometry
 386 (Location in Fig. 3 – IS4).

387 Dike geometry (attitude, thickness, and wall shape) varies according to the area where they
 388 intruded into the pluton. These variations were analyzed on five inselbergs, selected for detailed
 389 study (see section 2.3), and are hereinafter presented according to the inselberg location on the
 390 pluton.

391 4.2.2.1 *Inselbergs in the southwest part of the pluton*

392 Within the IS1 inselberg (Fig. 8), 432 outcropping dike surfaces were traced based on the
 393 high-resolution orthophoto. The black lines on the DEM (Fig. 8A) correspond to the
 394 intersection between the dike and the slope of the inselberg; that is, they represent only the
 395 superficial identification of dike outcrops.



396

397 Fig. 8. Geomorphological features of the IS1 inselberg, located in the SW part of the Quixadá Pluton.
 398 A – digital surface model with dike outcrops (black lines). The stereographic projection (a1) shows the
 399 tendency of low dip angles of dikes measured in this area; B – photo of the northern hillside of IS1,
 400 where a sub-horizontal dike set occurs. Location of inselberg in Fig. 3.

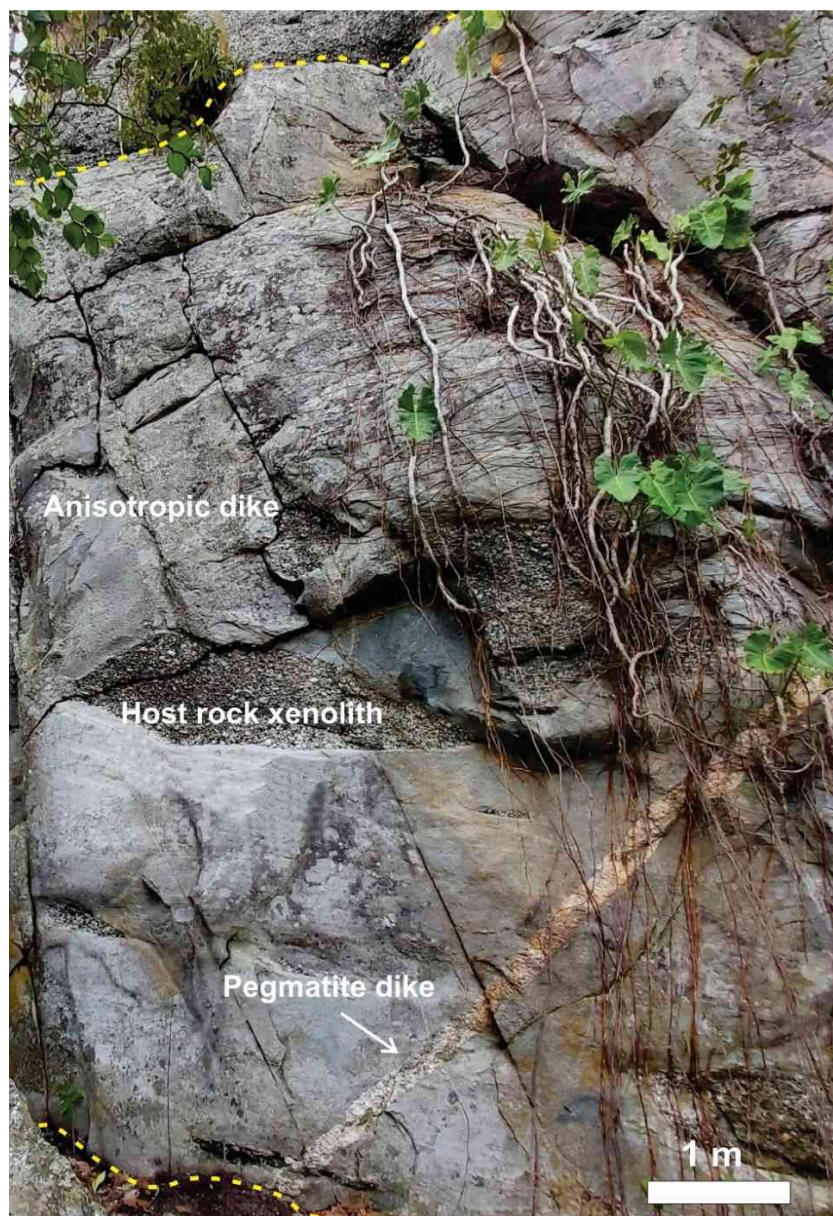


401

402 Fig. 9. Example of a sub-horizontal dike array exposed in straight vertical walls in the IS1. A large
 403 tafone (20 m x 10 m) is seen in the foreground, with the roof constrained by the dike. Multiple
 404 weathering pits dot the top surface of the inselberg. A – The zoomed photograph evidences the
 405 rectilinear wall geometry of the dike, marked by a sharp contact with the host rock and consistency of
 406 dike thickness. Location in Fig. 3 – IS1.

407 The dike set is composed of gently inclined bodies, with dip angles ranging from 8° to 34°,
 408 dipping to NW and SE, forming a sub-horizontal pattern typical for dikes in the SW sector of
 409 the pluton (Fig. 9). The dikes exhibit rectilinear walls and sharp contacts with the host rock
 410 (Fig. 9A1); a consistent dike thickness usually characterizes this type of geometry. Vertical

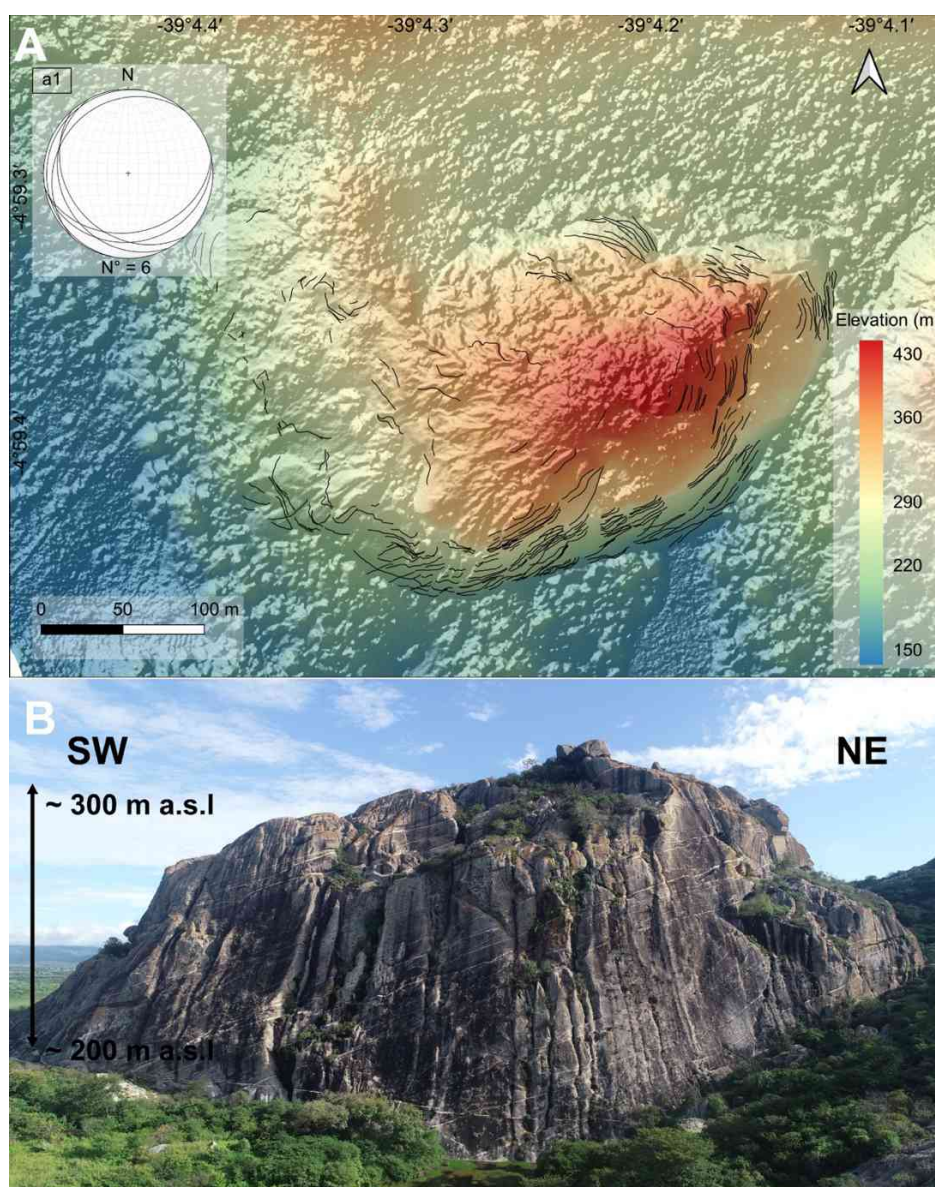
411 joints are developed in the peaks of IS1, locally intersecting low-angle dikes. These fractures
412 usually facilitate the collapse of blocks, favoring the steep and angular slope shape. The
413 foreground of Fig. 8B shows the portion of the inselberg with better development of vertical
414 fractures; in other parts, their occurrence is less evident and they usually control only minor
415 features of mechanical breakdown.



416

417 Fig. 10. 6m-thick Anisotropic dike (AD), displaying roughly vertical superficial joints and cut by a late
418 pegmatite dike. The yellow dotted lines mark the boundary surfaces of the dike AD. Location in Fig. 3
419 - IS1.

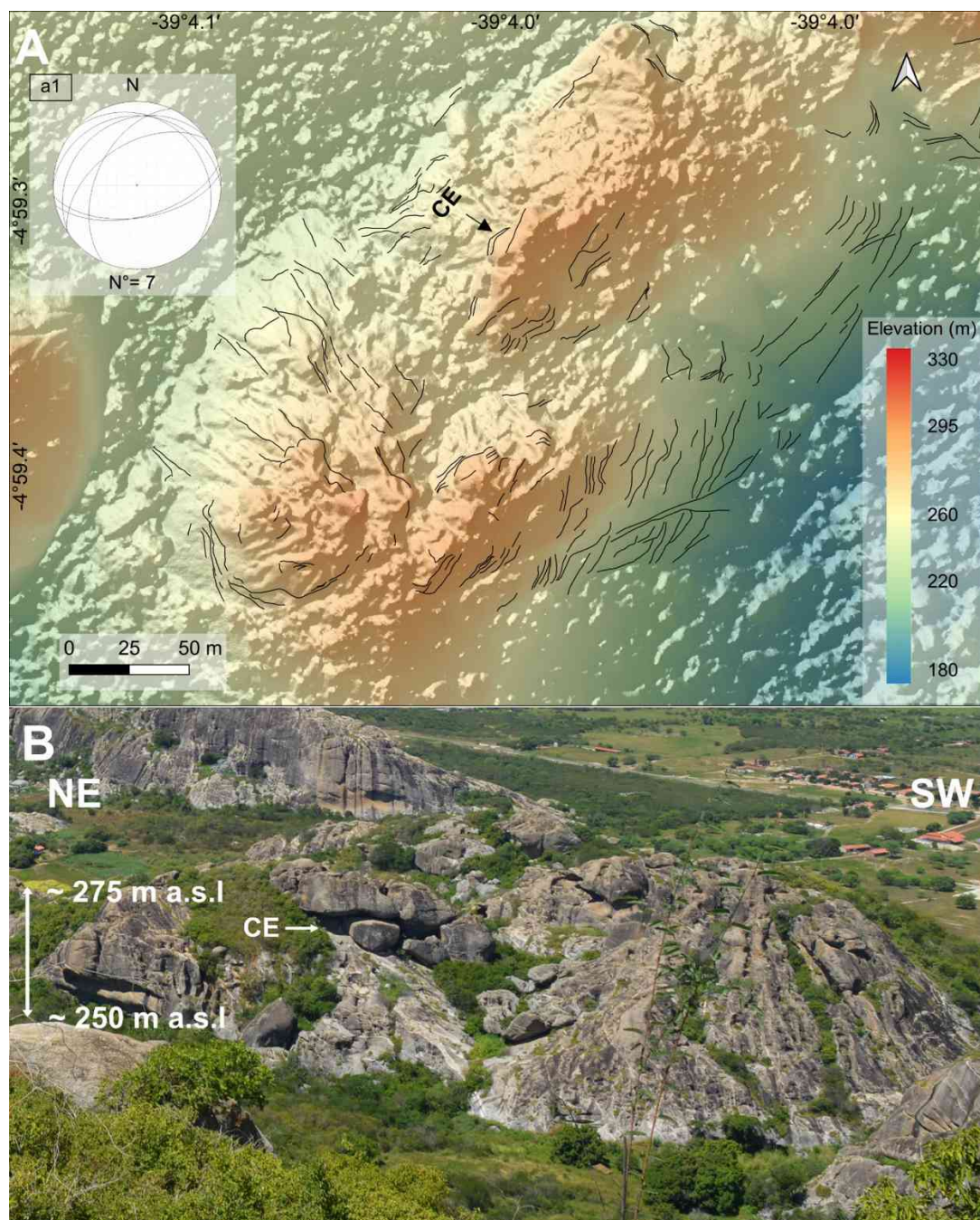
420 Besides felsic dikes, anisotropic dikes also occur in this inselberg, but not in a swarm similar
 421 to FgP and CgP. In contrast, they are found as large intrusions (up to 6 m thick), which are older
 422 than the pegmatite granite dikes since they are cut by them (Fig. 10). In addition, angular
 423 boulders (up to ca. 4 m long) are commonly found near the intrusions, suggesting fracture and
 424 rockfall of dike fragments.. They are particularly abundant in the SW part of the pluton.



425

426 Fig. 11. Geomorphological features of the IS2 inselberg, SW of the Quixadá Pluton. A – digital surface
 427 model of the inselberg with mapped dikes (black lines). The stereographic projection (a1) illustrates the
 428 low dip of the dikes; B – southern hillslope of the inselberg, with a set of sub-horizontal dikes. Location
 429 of inselberg in Fig. 3. Note that megakarren features, which are continuous grooves in the slopes
 430 developed from the summit to the base of the inselbergs and are colonized by dark-colored lichens, give
 431 the impression of shading, so that they may resemble vertical fractures.

432



433

434 Fig. 12. Geomorphological features of the IS3 inselberg, SW of the Quixadá Pluton. A – digital surface
 435 model with dike outcrops (black lines). The stereographic projection (a1) shows variable dip angles of the
 436 dikes; B – oblique northeastern view of the inselberg. An arrow indicates the entrance (CE) to a
 437 large rock overhang (cave). Location of inselberg in Fig.3.

438 Figure 11A shows the mapped dike outcrops (346) within the IS2 inselberg. Their general
 439 pattern is similar to the array on IS1. Dip angles range from 4° to 31° , hence accounting for a

440 sub-horizontal array, and dip directions are to the W and SW. Large anisotropic dikes have not
441 been found.

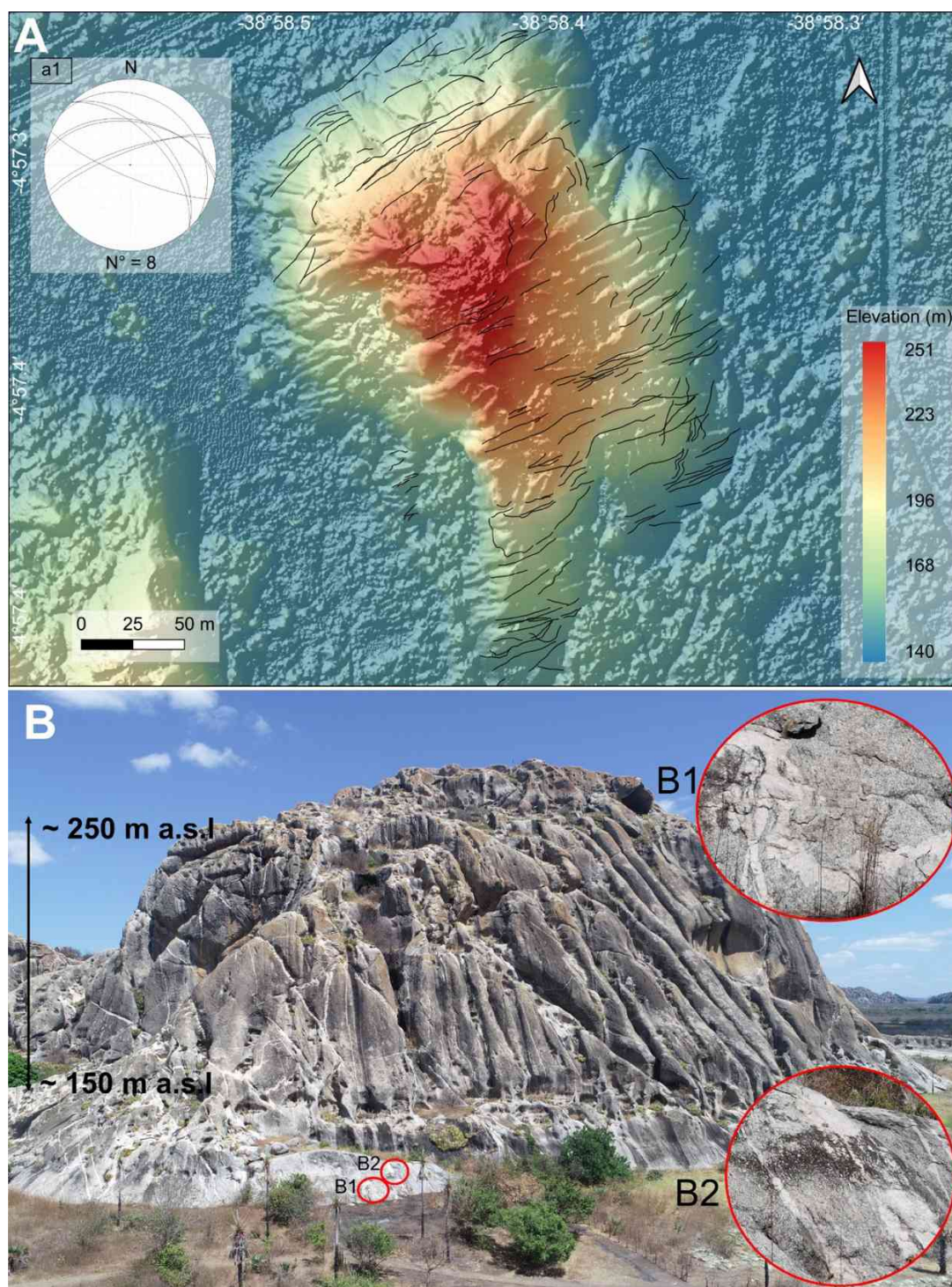
442 Within the IS3 inselberg, 308 dikes were identified (Fig. 12). Intersection lines of the dikes
443 are predominantly rectilinear, with a few dikes of deformed geometry expressed by a sigmoidal
444 shape. Dip angles range from 18° to 59°, and dips are preferentially to the NW and S, including
445 low- and medium-angle dikes. Metric fragments of anisotropic dikes (boulders) occur within
446 the northern talus deposit at the footslope, between the three inselbergs described here in detail.
447 At several places, exposed dike planes coincide with the top surface of the inselberg, whereas
448 within the large rock overhang (Fig. 12B), part of the cave ceiling is delimited by a felsic dike.

449 *4.2.2.2 Inselbergs in the eastern part of the pluton*

450 In the eastern part of the Quixadá Pluton, the pattern of dike swarms becomes more complex
451 since dike intersections are more frequent than in the dike arrays described in the SW part and
452 due to a generally wider variation in dike attitudes. Additionally, cross-cut relationships of a
453 sub-vertical and sub-horizontal sets were identified.

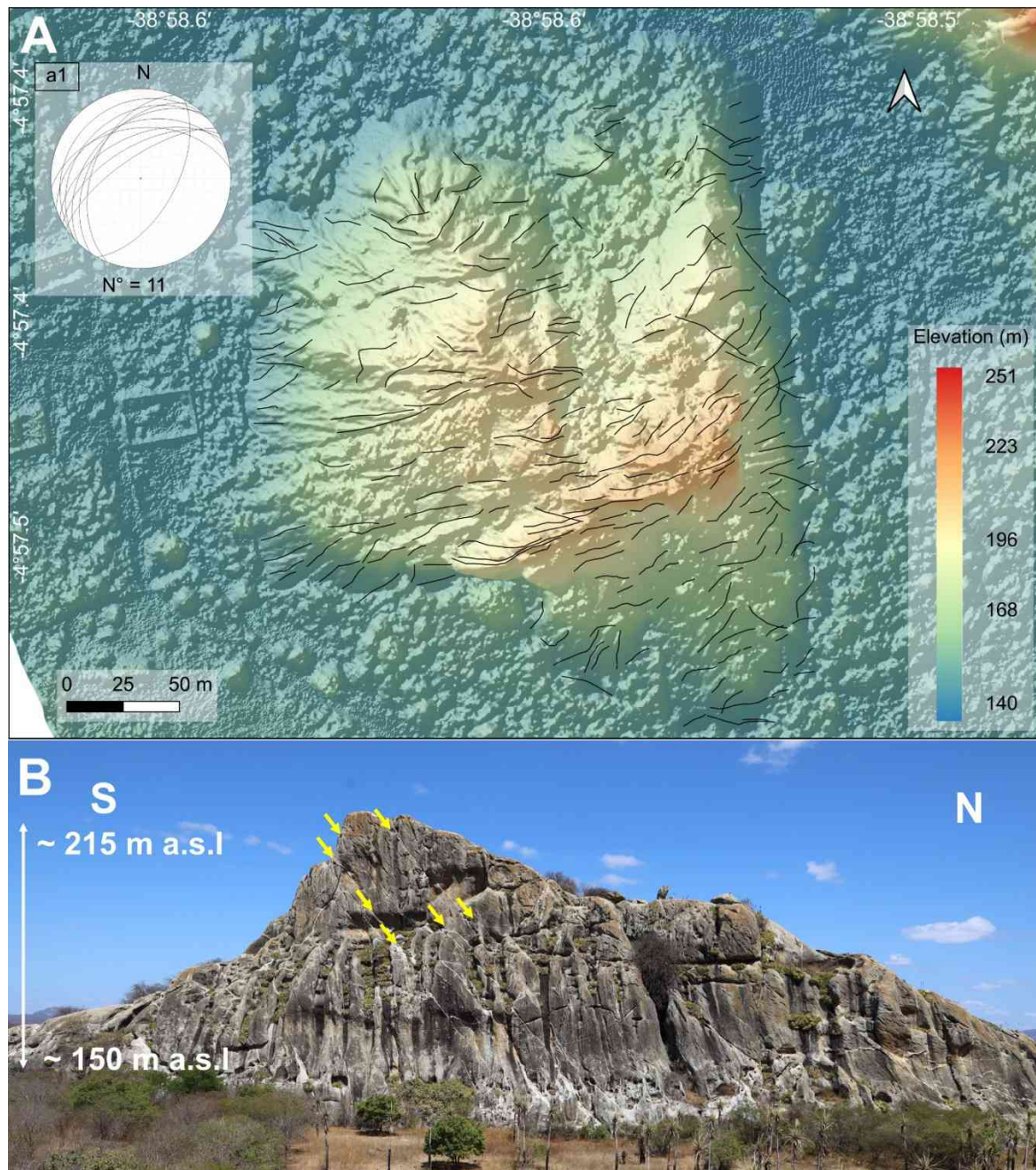
454 Within the IS4 inselberg, 310 dike outcrops were traced (Fig. 13). Dike wall geometry is
455 characterized by rectilinear and sharp contacts; occasionally deformed dikes of irregular shape
456 (Fig. 13-B1) and dikes with gradational borders are observed (Fig. XB2) Non-rectilinear dikes
457 present irregular thickness and, sometimes, are difficult to evaluate consistently. The range of
458 dip angles is wider than that of the dike array in previous inselbergs, varying from 21° to 77°,
459 encompassing more than one dike set. Dips are preferentially to the N and NE. A sub-vertical
460 array dominates on average, although both low- and high-angle dikes compose the set.

461 The IS5 inselberg shows 97 dike outcrops (Fig. 14). Dike wall geometry is similar to the
462 dikes on IS4, with both rectilinear and deformed dike walls present. This similarity reinforces
463 the contrast in the dike arrays between the eastern and southwestern sectors of the Quixadá
464 Pluton. The dikes also display a large range of dip angles, from 17° to 70°, dipping mainly
465 towards the NW and W. The average dip angle is 45°, and most measurements are below the
466 average (detailed data shown in Supplementary Material D). Several medium-angle dikes tend
467 to form a sub-parallel array and are intersected by steeply-dipping dikes. It is worthwhile noting
468 that the inselberg displays an asymmetry on the slope that coincides with the trend of dike
469 attitudes (see Fig. 17 in the discussion section).



470

471 Fig. 13. Geomorphological features of the IS4 inselberg, in the E sector of the Quixadá Pluton. A –
 472 digital surface model with the mapped outcropping dike surfaces (black lines). The stereographic
 473 projection (a1) shows medium to high dip angles of dikes; B – runnels, minor solution features, and
 474 occasional tafoni on the east-facing steep slope of the inselberg. Deformed dikes with irregular dike
 475 walls (B1) and dikes with gradational contacts (B2) are illustrated. Location of inselberg in Fig. 3.



476

477 Fig. 14. Geomorphological features of the IS5 inselberg, in the E sector of the Quixadá Pluton (Fig. 3,
 478 area B). A – digital surface model with dike outcrops (black lines). The stereographic projection (a1)
 479 shows dike dip angles; B – steep east-facing slope, with a concentration of medium-angle dikes with
 480 consistent attitudes (indicated by yellow arrows). Location of inselberg in Fig. 3.

481 4.3. Features associated with differential weathering of felsic dikes and host rock

482 Fracture planes have formed along the dike margins due to the discontinuity of the rock mass
 483 produced by the intrusion. Consequently, differential weathering features associated with

484 chemical dissolution (e.g., microcavities) or mechanical disintegration typically occur at the
 485 interface between the dikes and the host rock. Other weathering and erosional features are
 486 limited to a space available between two parallel dikes, suggesting a constraining role of felsic
 487 dikes with respect to hillslope degradation. Further, rock mass fragmentation into individual
 488 blocks occurs due to fracture propagation along individual dikes.

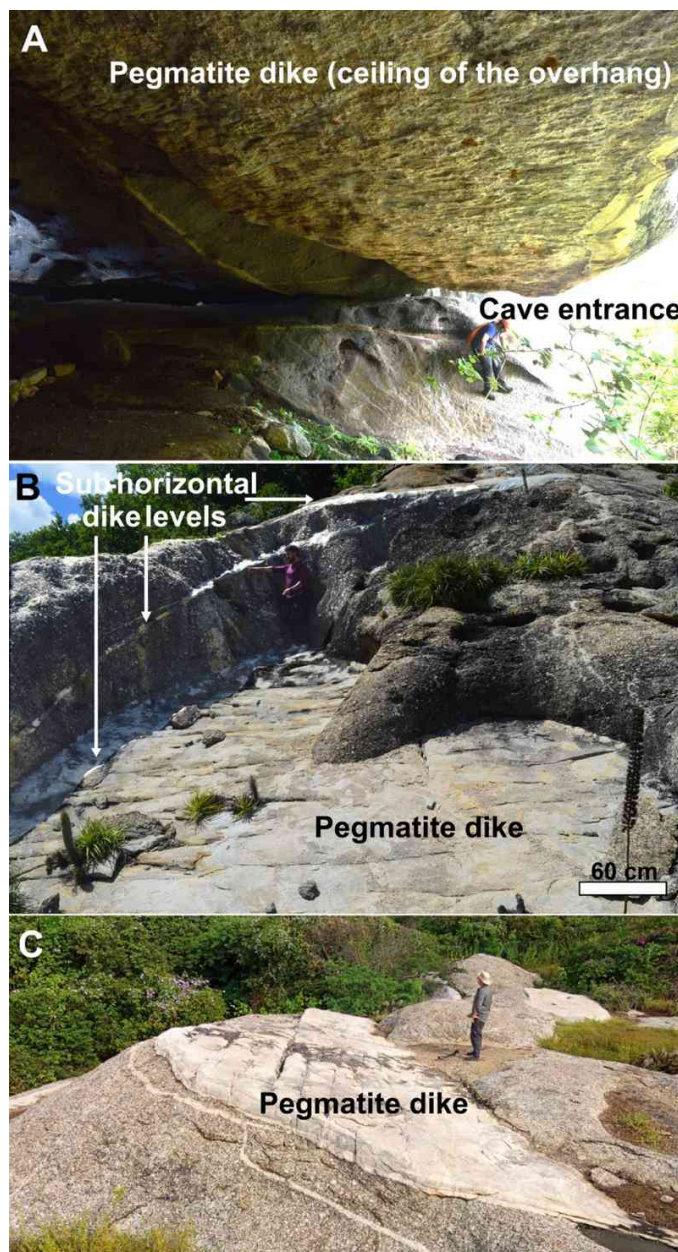


489

490 Fig. 15. Typical differential weathering features on the pegmatite/porphyritic monzonite interface. A –
 491 fine-grained pegmatitic dike (FgP) protruding from the host rock; B – karren developed in the host rock
 492 between parallel felsic dikes; C – dissolution runnel along a 60° dipping dike – host rock contact; D –
 493 fracture along the dike-host-rock boundary. Location in Fig. 3 – IS1.

494 The most frequent minor features on inselbergs of the Quixadá Pluton associated with dikes
 495 are: dikes protruding a few centimeters from the porphyritic host rock (Fig. 15A); dissolution
 496 features developed on the host rock between parallel dikes (Fig. 15B); alveoli, weathering pits,
 497 and dissolution runnels coincident with the dike margins (Fig. 15C); and fractures along the
 498 dike walls accounting for the fragmentation of blocks; in places, vegetation grows and expands
 499 the fracture (Fig. 15D). These features are particularly associated with pegmatite dikes, which

500 usually protrude above the host rock surface, suggesting higher resistance against weathering.
 501 The dikes and host rock surface present signs of alteration, such as roughness and fracturing.
 502 However, it is the host rock that concentrates the majority of dissolution features, most of them
 503 initiated by the dissolution of the mafic portions of the rock.



504

505 Fig. 16. Features related to the resistance of gently dipping pegmatite dikes and consequent exposure of
 506 dike boundary surfaces. A – pegmatite dike coincides with the ceiling of a large overhang developed in
 507 porphyritic monzonites (inselberg IS3). B – Sub-horizontal dike creates the floor of a large weathering
 508 pan (inselberg IS3). C – gently-dipping pegmatite dike accounts for the top surface of a residual granite
 509 hill. Note subparallel joints on the surface of the dike in B and C. Location of in Fig. 3.

510 An important factor controlling the type of features developed on the margins of the dikes is
511 their geometry, particularly the dip. For instance, dissolution runnels are incised preferentially
512 along discontinuities promoted by steeply-dipping dikes (Fig. 15C). In contrast, mostly sub-
513 horizontal dikes were identified as protrusions from the host rock (Fig. 15A). Sub-horizontal
514 dikes have their boundary surfaces exposed as parts of the morphological surface, clearly as a
515 result of former erosion of the host rock, evidencing contrasting resistance to weathering (Fig.
516 16). For example, Fig. 16A presents a gently-dipping (ca. 20°) pegmatite dike forming part of
517 the ceiling of a large overhang, formed in the porphyritic granite facies, whereas Fig. 16B shows
518 that the sloping floor of a large weathering pit (pan) is made of a pegmatite dike dipping at 35°,
519 which halts further deepening of the pan and forces its lateral expansion. It can also be observed
520 the sub-horizontal arrangement of the dikes at the hillslope scale. At a larger spatial scale of
521 tens of meters dip direction of a dike (Fig. 16C, to the right), and the slope inclination may
522 coincide, promoting conformity between the outline of the relief and dike geometry.

523 **5. Discussion**

524 Tectonic setting and lithology are regional-scale driving factors of granite landform
525 evolution (Migoñ, 2004, 2006). First, concerning the tectonic framework, the Quixadá inselberg
526 field is located in the South American Passive Margin, with a limited role played by differential
527 uplift and subsidence along faults (Maia and Bezerra, 2020). Second, the inselbergs in the
528 Quixadá Pluton are built of granitic rocks and rise from an erosion surface developed in the
529 same general lithology (Maia et al., 2015; Costa et al., 2020). Thus, they are not lithologically-
530 controlled landforms. In addition, no relief differentiation is promoted directly by the
531 lithological contact of the pluton with its country rocks (Fig. 1).

532 The gross petrological uniformity of hill-plain complexes was argued by Twidale (1971),
533 who highlighted the structural diversity within inselberg landscapes, which acquires
534 geomorphological significance (Migoñ, 2006), especially in relatively stable tectonic settings
535 and within protracted periods of geomorphic evolution. In the Quixadá area, subaerial evolution
536 of the denudational landscape has occurred since at least Cenozoic (Peulvast and Claudino
537 Sales, 2004). The structures observed in this study consist of subtle foliation and felsic dike
538 swarms, which combine structural and compositional aspects significant for rock control.

539

540

541 *5.1. Controls of dike geometry on inselberg morphology*

542 The geometry of brittle deformation structures such as dikes and veins within the Quixadá
543 Pluton was reported by Nogueira (2004), whose data are consistent with our observations on
544 the variable strike and irregular distribution of dikes within the granitic body, with a particular
545 abundance in the SW sector. Variations in the distribution and geometry of dikes and veins
546 often occur in granitoid intrusions and reflect the deformational setting during the emplacement
547 (Hoek, 1991; Druguet et al., 2008).

548 The presented results show a distinction between sub-horizontal dikes with rectilinear walls
549 (SW part of the pluton) and multidirectional dike arrays with dikes of varied geometry, from
550 sharp contacts to gradational borders (mostly in the E part of the pluton). The change in dike
551 geometry of Quixadá pegmatites has been reported as a function of melt fractionation during
552 intrusion (Almeida, 1995), as bodies emplaced with low melt fraction tend to exhibit sharp
553 contact with the host rock, while dikes intruded with high melt fraction present less planar walls.

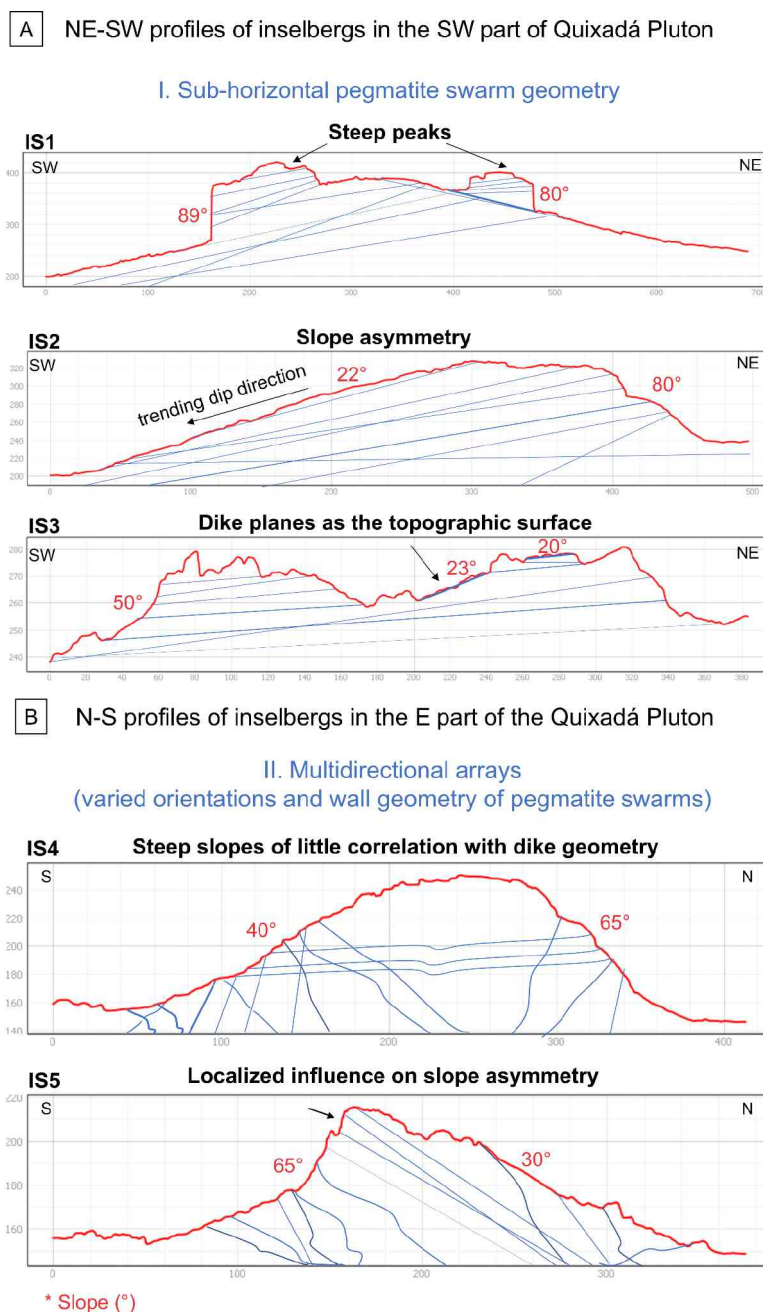
554 Changes in dike wall geometry and dike orientation were observed to exert structural control
555 on morphological aspects of inselbergs. Subparallel and sub-horizontal dikes tend to promote
556 less fractured slopes, resulting in sharply pointed peaks, such as in IS1 (Fig. 17A). In these
557 cases, the horizontal fractures into which dikes have intruded do not promote slope instability.
558 Although vertical joints are present in IS1, they are mostly responsible for small rockfalls and
559 the array of sub-horizontal dikes tends to constrain further development of vertical fracturing.

560 It is important to note that the role of joints, especially unloading or sheet joints of curved
561 geometry, has been argued as likely responsible for the domical shape of inselbergs and
562 bornhardts (Twidale, 1981; Twidale and Vidal-Romani, 2005). Although the occurrence of
563 mostly thin slabs may be identified on the inselbergs of the Quixadá area, the hills themselves
564 do not seem to have their present-day slope outlines controlled by sheeting joints, and one
565 interesting aspect of Quixadá inselbergs is that they exhibit a variety of morphologies other
566 than the classical domical shape. One evident reason is the control that other structures - such
567 as dike swarms - exert on the shapes of inselbergs.

568 Slope asymmetry (e.g., IS2) (Fig. 17A) is an example of how consistent dike orientations,
569 expressed by trends of dip and dip direction ($\sim 20^\circ$), correlate with the slope angle ($\sim 22^\circ$), such
570 that the morphology of the inselberg conforms to the geometry of the dike array. Moreover,

571 when dike planes form the topographic surface of inselbergs due to erosion of the host rock, the
 572 outline of the slope also tends to reflect dike orientation (e.g., IS3).

573

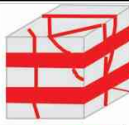

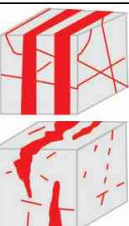


574

575 Fig. 17. Topographic profiles showing morphological aspects of inselbergs in relation to pegmatite
 576 swarm arrangements (y-axis: altitude; x-axis: length in meters). A – NE-SW profiles of inselbergs in the
 577 SW part of the Quixadá Pluton, illustrating controls of sub-horizontal pegmatite geometry on slope
 578 features. B – N-S profiles of inselbergs in the E part of the Quixadá Pluton, where multidirectional arrays
 579 are frequent and structural control on hillslope morphology is less evident.

580 Multidirectional dike swarms of varied geometry in terms of dip angle (wider range) and
 581 wall geometry (rectilinear and deformed dikes forming a swarm) are characteristic of the
 582 eastern sector. In this area, rectilinear dikes, if dipping by more than 60° , tend to guide the
 583 incision of dissolution features. In contrast, deformed dikes do not create extensive fracture
 584 planes or exert any clear control on inselberg morphology (e.g., IS4), analogous to those
 585 controls identified in the SW part of the pluton.

586 As these swarms show a complex array, subsets of rectilinear dikes with consistent attitudes
 587 may still exert local control on hillslope morphology, such as the massiveness of less fractured
 588 sectors and slope inclination according to dike geometry (e.g., IS5). Notwithstanding, the
 589 absence of preferential dipping in multidirectional arrays diminishes the direct control of dike
 590 geometry on inselberg morphology. This reduced control is likely a result of an increased
 591 representation of dikes with ductile geometry (as named by Kjoll et al., 2019), which lack a
 592 clear structural discontinuity along the interface with the host rock in the form of a fracture
 593 plane in their walls (as seen in rectilinear dikes).

INTERPRETATIVE CHART OF DIKE CONTROL ON INSELBERG MORPHOLOGY				
EMPLACEMENT SETTING	DIKE SWARM GEOMETRY		DEGREE OF ROCK CONTROL	GEOMORPHOLOGICAL RESPONSE
	DIP ANGLE RANGE	DIKE/ HOST R. CONTACT		
A 	Low to medium-angle dikes ($<45^\circ$)	Sharp contacts and rectilinear walls	+	A Pegmatite swarms supporting: <ul style="list-style-type: none"> • Less fractured peaks • Massive inselberg slopes Individual dike planes forming: <ul style="list-style-type: none"> • Base level of weathering pits • Ceiling of large overhangs • Topographic surface of inselbergs
B 	High-angle dikes ($>45^\circ$)			B Incision of dissolution runnels along dike-host rock contact
C 	Multi-directional arrays (dikes up to 77° and with less defined planes).	Transition from sharp to gradational contacts and undulating shapes	-	C No direct control on inselberg morphology (Only rectilinear dike subsets promote localized controls)

594

595 Fig. 18. Interpretative chart of dike control on inselberg morphology. Two main trends are established.
 596 The brittle dike swarms (A and B) promote direct control at the feature and landform scales. Structural
 597 control becomes less evident in multidirectional dike arrays (C), and mainly localized dike subsets exert
 598 control on morphology. Emplacement setting modified from pegmatite orientation models in Brisbin
 599 (1986).

600 Regarding the orientation of pegmatite sets, Brisbin (1986) proposed models of pegmatite
601 intrusion correlating dike orientation with the rheological state of an isotropic host rock.
602 Accordingly, sub-horizontal and subparallel fracture sets are favored in brittle domains with a
603 minimum vertical stress. With increasing depth and conditions of transition to a ductile domain,
604 pegmatites tend to intrude in vertical fractures.

605 From the above discussion of the morphological influence of pegmatite swarm geometry,
606 we propose an interpretative chart based on the variations of pegmatite dike orientation
607 according to the rheological state (following Brisbin, 1986), dike arrangement, and typical
608 geomorphological response to these structural factors found on the studied inselbergs (Fig. 18).

609 *5.2. Rock control at the detail scale*

610 *5.2.1. Diversity of host rock and dikes as factors guiding selective weathering*

611 Our results regarding the composition of three types of felsic dikes in the Quixadá Pluton
612 are consistent with earlier studies (Silva, 1989; Torquato et al., 1989). The dikes promote
613 textural, compositional, and structural bedrock discontinuities in relation to their host rock,
614 accounting for local changes in the mechanical behavior of the rock mass (Turichshev and
615 Hadjigeorgiou, 2017). The primary textural contrast occurs within the porphyritic rocks,
616 between the matrix with a high proportion of mafic content and the potassium feldspar
617 megacrysts. This partially accounts for the lower average of mechanical strength of the host
618 rock due to the contrast in the strength of more felsic and mafic portions of the host rock.
619 Regarding the latter aspect, Le Pera and Sorriso-Valvo (2000) stated that biotite content is a
620 key factor influencing the mechanical behavior of granitoid outcrops and their degree of
621 weathering. Also, the heterogeneous texture promotes differential mineral weathering within
622 the rock and granular disintegration (Migoń, 2006). Geochemical data attest to the preferential
623 susceptibility of the host rock and mafic enclaves to chemical weathering, as they yield the
624 highest FeO_t and MgO contents among the granitic facies of the Quixadá Pluton. As a result,
625 various dissolution features such as pitting, alveoli, tafoni, honeycombs, and weathering pits
626 tend to initiate at the low-strength mafic portions of the groundmass or at the mafic enclaves,
627 corroborating earlier works on granite terrains (Migoń, 2006; Maia et al., 2015; Eggleton, 2017,
628 2021).

629 More importantly, our results suggest that felsic dike intrusions generate conspicuous
630 discontinuities revealed by: (i) compositional heterogeneity due to their higher SiO₂ content;
631 (ii) textural contrast since the dikes vary from fine- to coarse-grained; and (iii) subtle strength
632 variation, as UCS average values obtained from dike surfaces are generally higher than those
633 from the host rock. These factors account for the development of a plane of weakness at the
634 dike/host rock interface, which becomes a preferential zone for fracturing and selective
635 weathering (Ortega et al., 2014; Place et al., 2016).

636 Selectivity of weathering associated with dikes was particularly observed when pegmatite
637 dikes hindered the enlargement of dissolution processes initiated in the host rock. Similar
638 findings regarding cavernous weathering associated with dike-related discontinuities were
639 recently reported by Maia et al. (2022). These authors also stated that dikes are directional
640 constraints of fracturing, an expected outcome since dikes are fluid-filled fractures (Pollard and
641 Townsend, 2018). In regard to fracturing behavior, Shang (2020) pointed out that fracturing
642 along the dike-host rock interface occurs mainly when the dike is generally more resistant than
643 the host rock, consistent with our observations. Higher resistance of dikes is usually evidenced
644 by dike protrusions, typically associated with siliceous intrusions worldwide. Examples include
645 observations of several fine- to medium-grained granitic and syenitic dikes with >65% SiO₂
646 (Catingueira dikes) that stand out from the Cachoeirinha metasediments (phyllites) in NE Brazil
647 (cf. Sial, 1986; Ferreira and Sial, 1986); studies of microweathering on glacial outcrops, with
648 protrusions of quartz and aplite veins above the host rock (Dahl, 1967; Clement et al., 1976;
649 André, 2002); and the presence of felsic dikes up to 30 m thick forming ridges in the Spanish
650 Peaks (USA), whereas the host rock is lowered and mafic dikes are excavated to form trenches
651 (Johnson, 1968).

652 Rock composition is a key aspect in these examples. Our results suggest that geochemistry
653 is the outstanding factor in dike resistance, especially due to the high quartz content, as
654 proposed by Nicholson (2008). Thus, although fine-grained granites may be considered more
655 resistant due to their tight fabric (Migoñ, 2006; Migoñ and Vieira, 2014), no significant strength
656 variability was found between FgP and CgP, and the features presented are associated with both
657 types. Besides the silica content, the K₂O percentage (partly indicative of the presence of
658 potassium feldspar) is slightly higher in dikes than in the host rock. Some authors pointed out

659 that potassium-rich granitoids are relatively more resistant than calcium-rich ones (Pye, 1986;
660 Migoñ, 2006; Eggleton, 2017), providing chemical resistance, especially to pegmatites.

661 In contrast to pegmatitic dikes, anisotropic dikes appear more prone to fracturing and
662 fragmentation, as illustrated by their occurrence within talus slopes in the form of loose
663 boulders. This tendency towards faster mechanical disintegration can be partially interpreted as
664 a result of (i) their lower silica and higher FeO_t content than in the pegmatite granite dikes and
665 (ii) their anisotropic fabric, marked by the primary lineation of minerals. A slight decrease in
666 surface strength attests to these characteristics. Compositional influence on mechanical
667 behavior of dikes was argued by Turichshev and Hadjigeorgiou (2017), and textural
668 anisotropies by Williams and Robinson (1983). The interplay of these aspects may drive the
669 response to mechanical and weathering processes.

670 5.2.2. The role of lithological contacts

671 In dikes with sharp contacts with the host rock, also named brittle dikes (Kjoll et al., 2019),
672 a fracture plane is created, and the emerging structures account for anisotropy and promote
673 erosion (Beavis, 2000). Previous studies strongly suggested that the geometry and orientation
674 of brittle structures influence fracture propagation and consequent mechanical disintegration
675 within rock masses (Turichshev and Hadjigeorgiou, 2017). Here we call attention to this
676 relationship concerning changes in dike dip in the studied pegmatites.

677 We identified numerous dissolution runnels preferentially incised along the contact of high-
678 angle dikes (>60°) with the host granite. Similar control was observed on steeply-dipping dikes,
679 tending to be better exposed than those dipping at low angles (Gans and Gentry, 2016). This
680 relationship was also mentioned by Beavis (2000), who claimed that steeply dipping structures
681 tend to guide runoff and hence, erosion.

682 By contrast, sub-horizontal dikes typically appear as resistant features decelerating the
683 development of such rock degradation features as overhangs (upward growth hindered by a
684 resistant roof) and weathering pits and pans (deepening halted by a resistant floor). In these
685 cases, weathering is constrained by this low-dip discontinuity, revealing the structural geometry
686 of a dike. The correlation between dike dip and the shape of minor landforms was demonstrated
687 by Maia et al. (2022), who showed that the inclination of tafoni floors developed near
688 pegmatites was consistent with their dip angles, attesting to the direct control of dike geometry
689 on geomorphology.

690 5.3. Implications of dike swarm geometry on differential denudation and landform evolution

691 The geomorphic evolution of granite terrains, and the origin of granite inselbergs in
692 particular, used to be widely debated in the second half of the 20th century (see Duszyński et
693 al., 2022), but afterward the interest diminished, despite the growing availability of remotely
694 sensed topographic data and the development of various analytical techniques. With respect to
695 inselbergs, two conceptual models developed in the 1950s to 1970s continued to provide a
696 template for subsequent studies, with increasing evidence in favor of the etching/stripping
697 model, especially applicable to humid and semi-humid tropics (Thomas, 1978).

698 The two/multi-stage scenario offered a good answer as to *how* inselbergs originated and
699 evolved, whereas the question ‘why’ remained open. Reasons for the emergence of inselbergs
700 were mainly sought in structural characteristics, specifically jointing patterns, paying much less
701 attention to lithological factors. However, the latter is more prominent at the landscape scale
702 (Migoń, 1996, 2006; Godard et al., 2001; Eggleton, 2017, 2021). Even more so, dikes emplaced
703 within granite plutons were largely overlooked and considered site-specific curiosities rather
704 than factors of broader significance. They were typically presented as reasons for minor
705 ornamentations of exposed granite surfaces (Twidale, 1982; Pedraza et al., 1989).

706 The present-day morphology of the Quixadá inselberg field shows that steeply-dipping dike
707 sets are preferentially associated with features of water flow, as they form sub-vertical fracture
708 planes guiding weathering. Our observations are consistent with studies showing brittle
709 structures as guides for water percolation through basement discontinuities – including dikes,
710 veins, faults, and other rock anisotropies (Twidale and Campbell, 1993; Anderson and Bakker,
711 2008; Roques et al., 2014). As a result, fracture planes provide secondary permeability for the
712 otherwise solid and poorly permeable granite (Vidal-Romaní, 2008).

713 Considering that granite landforms typically evolve by multi-stage processes initiated in
714 subsurface conditions (Twidale and Vidal-Romaní, 1994) and accepting fracture geometry
715 control on surface processes (Beavis, 2000), we infer that systems of sub-vertical dikes and
716 fractures favor subsurface alterations, promoting the deepening of the weathering front.
717 Conversely, the sub-horizontal arrays of pegmatites, reported in this study as forming resistant
718 levels, will likely hinder weathering in sectors they are concentrated due to their roughly
719 perpendicular orientation with respect to vertical fracturing and consequent downward water
720 percolation. Since dike swarm geometry varies spatially, we infer that this contrast allows for

721 a gradual emergence of less altered sectors supported by resistant horizontal structures during
722 long-term differential denudation. Inselberg slopes built of massive granite in the SW part of
723 the Quixadá pluton are good examples of this control. Additionally, it was argued that systems
724 of steeply inclined fractures tend to enhance weathering adjacent to tors and steep-sided
725 inselbergs, leading to the origin of the surrounding plains (Linton, 1955; Twidale, 1971, 1998).

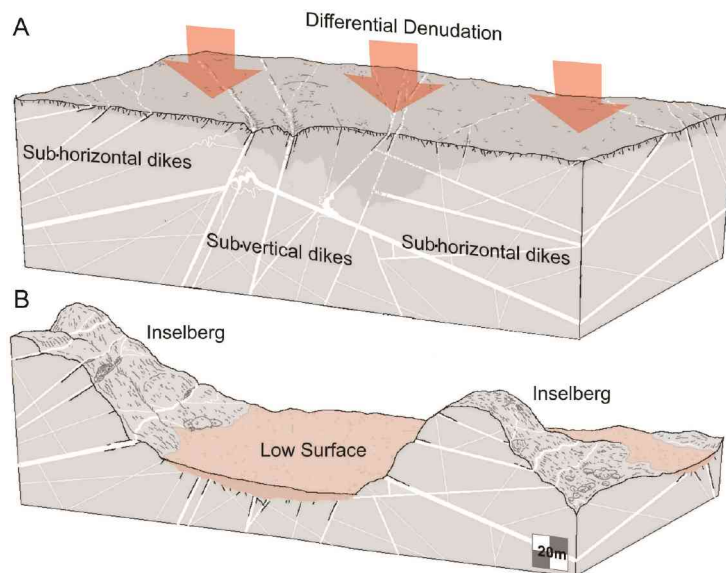
726 A question that can be raised is why vertical dikes do not remain in relief as a consequence
727 of their resistance since several studies addressing dike control in geomorphology referred to
728 ridge formation along individual, nearly vertical dikes (Johnson, 1968; Jürgens and Burke,
729 2000; Ernst and Buchan, 2004; Pedersen et al., 2010). However, these examples come from
730 igneous intrusions, which are hundreds of meters or kilometer-thick, not found in the Quixadá
731 Pluton. The pegmatites reported in this study are mainly centimeter-thick, and anisotropic dikes
732 reach a few meters. When the felsic dikes display sub-vertical orientation, the bordering host
733 rock is easily weathered, and the upstanding dikes start to fracture and lose stability. The
734 geometry of brittle structures influences the mechanical behavior of the rocks, as suggested by
735 several studies demonstrating that steeply dipping rock discontinuities tend to promote rock
736 failure when exceeding the friction angle, thus generating instability of slopes (Hoek and Bray,
737 1974; Brideau et al., 2009; Stead and Wolter, 2015; Vick et al., 2020).

738 Therefore, rock failures of different magnitudes are essential in the geomorphological
739 evolution associated with weathering and subsequent erosion of sectors with steeply dipping,
740 but not particularly thick dike swarms. We hypothesize that in the long-term steeply dipping
741 pegmatites will be eroded rather than form persistent ridges. In general terms, we infer that two
742 distinctive geometries of pegmatite swarms provide significant control over the evolution of
743 granite landscapes, and inselbergs in particular, resulting in contrasting surface expressions due
744 to differential denudation.

745 As shown in Fig. 19, the planes defined by the orientations of pegmatite dikes may pre-
746 condition erosion intensity by creating sub-vertical or sub-horizontal directional anisotropy.
747 The dikes, per se, constitute zones of increased resistance to erosion, particularly due to their
748 felsic composition (see Geochemistry Table in Supplementary Material A). Nonetheless, when
749 brittle, the dike/host rock interface forms a surface prone to the development of fracture planes,
750 in which all the secondary permeability concentrates and processes of chemical alteration and
751 loss of intergranular cohesion of the rock occur.

752 Since the mineralogy between the inselbergs and the surrounding plain within the Quixadá
 753 Pluton does not differ, the orientation of dike swarms becomes a significant factor guiding
 754 differential erosion. Dikes with high dip angles tend to favor fluid circulation, enhancing and
 755 focusing meteoric alteration. By contrast, low dip angles, which characterize the majority of
 756 pegmatite swarms in the Quixadá Pluton, favor neither water percolation nor alteration and
 757 block collapse, as the gentle inclination maintains rock blocks in place and piled up, despite
 758 being fractured. Where dike swarms intersect occasionally, local collapses might be generated,
 759 and cavities may form.

760 Therefore, planation and denudational surfaces are susceptible to structural control exerted
 761 by dike-related fracture planes. Accordingly, inselbergs are topographic manifestations of
 762 mechanical resistance nuclei of the granite pluton. This localized resistance is assumed to be
 763 strongly influenced by directional anisotropy of low dipping angles of dike swarms, halting
 764 weathering and rock disintegration on hillslopes, and guiding divergent erosion, which
 765 ultimately exposes the residual landforms such as the Quixadá inselberg field and the low-relief
 766 erosion surfaces in the surroundings.



767
 768 Fig. 19. 3D sketch model representing the relationships between the geometry of felsic dike swarms and
 769 differential denudation in the evolution of a granite landscape, based on the observations from the
 770 Quixadá inselberg field, NE Brazil. A – pre-exhumation phase, where weathering processes gradually
 771 take place guided by structures, particularly favored by sub-vertical dikes and related fractures. B –
 772 current topography results from differential erosion that allowed for the emergence of an inselberg
 773 landscape. These landforms are supported by granite rocks cut by sub-horizontal pegmatite swarms,
 774 which form resistant structures against erosion.

775 **6. Conclusions**

776 This paper demonstrated that dikes may play a significant role in the long-term evolution of
777 erosional granite terrains, particularly inselbergs. They differ from the host rock regarding
778 mineralogical composition, fabric and mechanical strength, whereas common sharp contacts
779 favor fracturing the rock mass along dike walls. However, relationships between dikes and the
780 morphology of granite landscapes are complex, reflecting a range of rock properties of
781 geomorphic significance and differences between dike-making rock and the host rock.

782 Key factors are the attitude of dikes, thickness, the density and geometry of dike arrays,
783 composition, fabric and hardness. Therefore, the presence of dikes in one place may increase
784 the susceptibility of the rock mass to weathering and erosion, whereas, in another, they may
785 decisively contribute to higher resistance. In the Quixadá Pluton investigated here, the dip of
786 dikes proves crucial. Lower dip angles increase the resistance, apparently because sub-
787 horizontal tabular bodies of resistant pegmatites forming the dikes act as effective barriers for
788 the downward progression of the weathering front. In addition, gently-dipping dikes hinder the
789 evolution of vertical fractures, which guide water percolation and weathering. Therefore, sub-
790 horizontal dike arrays also strengthen hillslopes of inselbergs, accounting for their considerable
791 steepness, and their geometry is often reflected by the inselberg morphology.

792 Apart from controlling large-scale geomorphic features, dikes are directly responsible for
793 various minor landforms such as ledges and protrusions, weathering pans and rock overhangs,
794 where they provide floors and ceilings, respectively, and split boulders. We also showed the
795 usefulness of UAV-based photogrammetry in capturing the spatial patterns of dikes, which are
796 very difficult to appreciate otherwise.

797 **Acknowledgments**

798 The authors are grateful for the resources for research obtained by the project Inselbergs de
799 Quixadá - Ceará - Brazil: Origin and Geomorphological Evolution by CNPq (National Council
800 for Technological Development Research) in Brazil. L.S and R.P.M would like to thank the
801 Capes-Cofecub programme for continuing support (Tc 981/20). We acknowledge useful
802 comments from two journal reviewers which helped us to improve the paper.

803

804 **References**

- 805 Almeida, A.R., 1995. Petrologia e aspectos tectônicos do complexo granítico Quixadá-Quixeramobim,
 806 CE (Doctoral dissertation). Instituto de Geociências, Universidade de São Paulo, São Paulo.
- 807 Almeida, F.F.M., Brito Neves, B.B., Carneiro, C.D.R., 2000. The origin and evolution of the South
 808 American Platform. *Earth-Science Reviews* 50, 77-111. [https://doi.org/10.1016/S0012-](https://doi.org/10.1016/S0012-8252(99)00072-0)
 809 [8252\(99\)00072-0](https://doi.org/10.1016/S0012-8252(99)00072-0).
- 810 Alvares, C.A., Stape, J.L., Sentelhas, P.C., Gonçalves, J.L.M., Sparovek, G., 2013. Koppen's climate
 811 classification map for Brazil. *Meteorologische Zeitschrift* 22, 711-728. [https://doi.org/10.1127/0941-](https://doi.org/10.1127/0941-2948/2013/0507)
 812 [2948/2013/0507](https://doi.org/10.1127/0941-2948/2013/0507)
- 813 Anderson, E.I. Bakker, M., 2008. Groundwater flow through anisotropic fault zones in multiaquifer
 814 systems. *Water Resources. Research* 44, W11433. <https://doi.org/10.1029/2008WR006925>.
- 815 André, M.-F., 2002. Rates of postglacial rock weathering on glacially scoured outcrops: (Abisko-
 816 riksgården area, 68°N). *Geografiska Annaler* 84A, 139-150.
- 817 Aragão, A.J.S., Gorayeb, P.S.S., Galarza, M.A., 2020. Magmatic and tectonic evolution of the Chaval
 818 Granite at the end of the Neoproterozoic, northwestern border of the Borborema Province. *Brazilian*
 819 *Journal of Geology* 50, 1-26. <https://doi.org/10.1590/2317-4889202020190089>.
- 820 Archanjo, C.J., Trindade, R.I.F., Bouchez, J.L., Ernesto, M., 2002. Granite fabrics and regional-scale
 821 strain partitioning in the Seridó belt (Borborema Province, NE Brazil). *Tectonics* 21, 1003.
 822 <https://doi.org/10.1029/2000TC001269>.
- 823 Aydin, A., 2009. ISRM Suggested method for determination of the Schmidt hammer rebound hardness:
 824 Revised version. *International Journal of Rock Mechanics and Mining Sciences & Geomechanics*
 825 *Abstracts* 46, 627-634. <https://doi.org/10.1016/j.ijrmms.2008.01.020>.
- 826 Bezerra, F.H.R., Nascimento, A.F., Ferreira, J.M., Nogueira, F.C., Fuck, R.A., Brito Neves, B.B., Sousa,
 827 M.O.L., 2011. Review of active faults in the Borborema Province, Intraplate South America —
 828 Integration of seismological and paleoseismological data. *Tectonophysics* 510, 269 – 290.
 829 <https://doi.org/10.1016/j.tecto.2011.08.005>.
- 830 Beauvais, A., Ritz, M., Parisot, J.-C., Bantsimba, C., 2003. Testing etching hypothesis for the shaping
 831 of granite dome structures beneath lateritic weathering landsurfaces using ERT method. *Earth*
 832 *Surface Processes and Landforms* 28, 1071–1080.
- 833 Beavis, S.G. 2000. Structural controls on the orientation of erosion gullies in mid-western New South
 834 Wales, Australia. *Geomorphology* 33, 59-72.
- 835 Brideau, M.-A., Yan, M., Stead, D., 2009. The role of tectonic damage and brittle rock fracture in the
 836 development of large rock slope failures. *Geomorphology* 103, 30-49.
 837 <https://doi.org/10.1016/j.geomorph.2008.04.010>.
- 838 Brisbin, W.C., 1986. Mechanics of pegmatite intrusion. *American Mineralogist* 71, 644-651.
- 839 Castro, D.L.C., Castelo Branco, R.M.G., Martins, G., Castro, N.A., 2002. Radiometric, magnetic, and
 840 gravity study of the Quixadá batholith, central Ceará domain (NE Brazil): evidence for Pan-
 841 African/Brasiliano extension-controlled emplacement. *Journal of South American Earth Sciences* 15,
 842 543–551.
- 843 Clement, B., Landry, B., Yergeau, M., 1976. Dechaussement postglaciaire de filons de quartz dans les
 844 Appalaches Québécoises: (région de Sherbrooke, Canada). *Geografiska Annaler* 58A, 111-114.

- 845 Costa, L.R.F, Maia, R.P., Barreto, L.L., Claudino-Sales, V., 2020. Geomorfologia do nordeste
846 setentrional brasileiro: uma proposta de classificação. *Revista Brasileira de Geomorfologia* 21, 185-
847 208. <http://dx.doi.org/10.20502/rbg.v21i1.1447>.
- 848 Costa, C., Alvarado, A., Audemard, F., Audin, L., Benavente, B. Bezerra, F.H., Cembrano, J., González,
849 G., Lopez, M., Minaya, E., Santibanez, I., Garcia, J., Arcila, M., Pagani, M., Pérez, I., Delgado, F.,
850 Paolini, M., Garro, H., 2020b. Hazardous faults of South America; compilation and overview.
851 *Journal of South American Earth Sciences* 104, 102837.
852 <https://doi.org/10.1016/j.jsames.2020.102837>.
- 853 Dahl, R., 1967. Post-glacial micro-weathering of bedrock Surfaces in the Narvik District of Norway.
854 *Geografiska Annaler* 49A, 155-166.
- 855 Druguet, E., Czeck, D.M., Carreras, J., Castaño, L.M., 2008. Emplacement and deformation features of
856 syntectonic leucocratic veins from Rainy Lake zone (Western Superior Province, Canada).
857 *Precambrian Research* 163, 384 - 400. <https://doi.org/10.1016/j.precamres.2008.02.001>.
- 858 Duszyński, F., Ford, D.C., Goudie, A.S., Migoń, P., 2022. Rock control in geomorphology. In: Burt,
859 T.P., Goudie, A.S., Viles, H.A. (Eds.), *The History of the Study of Landforms or the Developments*
860 *of Geomorphology*, vol. 5. Geological Society Memoir 58, 151–171.
- 861 Eggleton, R.A., 2017. Mineralogy maketh mountains: Granitic landscapes shaped by dissolution.
862 *Geomorphology* 285, 363-373. <https://doi.org/10.1016/j.geomorph.2017.01.016>.
- 863 Eggleton, R.A., 2021. Some factors affecting granitic pluton topography: Pluton topography in the
864 southern Lachlan Foldbelt. *Geomorphology* 381, 107643.
865 <https://doi.org/10.1016/j.geomorph.2021.107643>.
- 866 Ernst, R.E., Buchan, K., 2004. Dyke (Dike) swarm. In: Goudie, A. S. (Ed.), *Encyclopedia of*
867 *geomorphology*. Routledge, London, p. 305.
- 868 Ferreira, V. P., Sial, A. N., 1986. The peralkalic magmatism in the Precambrian cachoeirinhas-salgueiro
869 foldbet, Northeast Brazil: Geochemical aspects. *Revista Brasileira de Geociências* 16, 73 – 85.
- 870 FUNCEME - Fundação Cearense de Meteorologia e Recursos hídricos., 2022. Calendários de chuvas
871 no estado Ceará. <http://funceme.br/app-calendario/ano/municipios/media/20221> (accessed 11 Nov
872 2022).
- 873 Fossen, H., 2016. *Structural geology*, 2nd edition. Cambridge University Press, Cambridge.
- 874 Galindo, A. C.; Nascimento, M. A. L.; Medeiros, V. C. 2019. Classificação/nomenclatura de rochas
875 plutônicas com base em diagramas modais e químicos: um estudo para rochas granitoides no extremo
876 nordeste da Província Borborema. *Estudos Geológicos*, 29, 180-195.
- 877 Gans, P.B., Gentry, B.J., 2016. Dike emplacement, footwall rotation, and the transition
878 from magmatic to tectonic extension in the Whipple Mountains metamorphic core complex,
879 southeastern California. *Tectonics* 35, 2564-2608. <https://doi.org/10.1002/2016TC004215>.
- 880 Gill, R., 2010. *Igneous rocks and processes: a practical guide*. Wiley Blackwell, New Jersey.
- 881 Godard, A., Lagasquie, J.-J., Lageat, Y. (Eds.), 2001. *Basement Regions*. Springer, Berlin.
- 882 Gooneraman, H., Taisne, B., 2015. Magma transport in dikes, In: Sigurdsson, H. (Ed.), *The Encyclopedia*
883 *of Volcanoes*, 2nd Edition, Academic Press, pp. 215-224.
- 884 Halls, H., 1982. The importance and potential of mafic dyke swarms in studies of geodynamic processes.
885 *Geoscience Canada* 9, 145-154.
- 886 Hoek, E., Bray, J.W., 1974. *Rock Slope Engineering*, Revised third edition. Institution of Mining and
887 Metallurgy, London.

- 888 Hoek, J. D., 1991. A classification of dyke-fracture geometry with examples from Precambrian dyke
889 swarms in the Vestfold Hills, Antarctica. *Geologische Rundschau* 80, 233-248.
- 890 INMET – Instituto Nacional de Meteorologia, 2022. <https://clima.inmet.gov.br/temp> (accessed 11 Nov
891 2022).
- 892 Jerram, D., Petford, N., 2011. *The field description of igneous rocks*. John Wiley and Sons, New Jersey.
- 893 Johnson, R.B., 1968. *Geology of the Igneous Rocks of the Spanish Peaks Region Colorado*, United
894 States Government Printing Office, Washington.
- 895 Jürgens, N., Burke, A., 2000. The arid scenario: Inselbergs in the Namib Desert are rich oases in a poor
896 matrix (Namibia and South Africa), In: Porembski, S., Barthlott, W. (Eds.), *Vegetation of tropical
897 rock outcrops (Inselbergs): Biotic diversity of a tropical ecosystem*. Springer, Berlin, pp. 237 – 257.
- 898 Kjöll, H.J., Galland, O., Labrousse, L., Andersen, T. B., 2019. Emplacement mechanisms of a dyke
899 swarm across the brittle-ductile transition and the geodynamic implications for magma-rich margins.
900 *Earth and Planetary Science Letters* 518, 223-235. <https://doi.org/10.1016/j.epsl.2019.04.016>.
- 901 Kortenien, J., 2015. Dike (Igneous), In: Hargitai H., Kereszturi Á. (Eds), *Encyclopedia of Planetary
902 Landforms*. Springer, New York. https://doi.org/10.1007/978-1-4614-3134-3_112.
- 903 Le Pera, E., Sorriso-Valvo, M., 2000. Weathering and morphogenesis in a mediterranean climate,
904 Calabria, Italy. *Geomorphology*, 34, 251-270.
- 905 Lidmar-Bergström, K., 1989. Exhumed Cretaceous landforms in south Sweden. *Zeitschrift für
906 Geomorphologie NF, Supplement-Band* 89, 21-40.
- 907 Lima, G.M.P., Corrêa-Gomes, L.C., 2015. Itatim geomorphological site: Largest concentration of
908 inselbergs in Brazil. In: Vieira, B.C., Salgado, A.A.R., Santos, L.J.C. (Eds.), *Landscapes and
909 Landforms of Brazil*. Springer, Dordrecht, pp. 371–380. DOI 10.1007/978-94-017-8023-0_34.
- 910 Linton, D.L., 1955. The problem of tors. *Geographical Journal* 121, 470-487.
- 911 Maia, R.P., Nascimento, M.A.L., Bezerra, F.H.R., Castro, H.S., Meireles, A. J de A., Rothis, L. M.,
912 2015. Geomorfologia do campo de inselbergues de Quixadá, Nordeste do Brasil. *Revista Brasileira
913 de Geomorfologia* 13, 240-253.
- 914 Maia, R.P., Nascimento, M.A.L., 2018. Relevos graníticos do Nordeste Brasileiro. *Revista Brasileira de
915 Geomorfologia* 19, 373-389. <https://doi.org/10.20502/rbg.v19i2.1295>.
- 916 Maia, R. P., Bezerra, F. H. R., 2020. Structural geomorphology in Northeastern Brazil. *SpringerBriefs
917 in Latin American Studies*, Cham. <https://doi.org/10.1007/978-3-030-13311-5>.
- 918 Maia, R.P., Bastos, F.H., Waldherr, F.R., Nascimento, M.A.L., Auler, A.S., 2022. Breves considerações
919 sobre Tafoni em inselbergs: aspectos genéticos e morfoestruturais. *Revista Brasileira de
920 Geomorfologia* 23, 1792-1811. <https://doi.org/10.20502/rbg.v23i4.2090>.
- 921 Mariano, G., Sial, A.N., 1990. Coexistence and mixing of magmas in the late precambrian Itaporanga
922 Batholith, state of Paraíba, Northeastern Brazil. *Revista Brasileira de Geociências* 20, 101-110.
- 923 Migoñ, P., 1996. Evolution of granite landscapes in the Sudetes (Central Europe): some problems of
924 interpretation. *Proceedings of the Geologists' Association* 107, 25-37.
- 925 Migoñ, P., 2004. Structural landform, In: Goudie, A S. (Ed.), *Encyclopedia of geomorphology*.
926 Routledge, London, pp. 1007-1009.
- 927 Migoñ, P., 2006. *Granite Landscapes of the World*. Oxford University Press, New York.
- 928 Migoñ, P., Vieira, G., 2014. Granite geomorphology and its geological controls, Serra da Estrela,
929 Portugal. *Geomorphology* 226, 1-14. <https://doi.org/10.1016/j.geomorph.2014.07.027>.
- 930 Migoñ, P., Maia, R. P., 2020. Pedra da Boca, Pai Mateus, and Quixadá—three possible Key Geoheritage
931 Sites in Northeast Brazil. *Geoheritage* 12, 51. <https://doi.org/10.1007/s12371-020-00473-4>.

- 932 Nicholson, D.T., 2008. Rock control on microweathering of bedrock surfaces in a periglacial
933 environment. *Geomorphology* 101, 655-665. <http://dx.doi.org/10.1016/j.geomorph.2008.03.009>.
- 934 Nogueira, J.F., Morales, N., 1999. Geometria e Cinemática de diques e veios no Batólito de Quixadá –
935 CE. In: National Symposium of Tectonic Studies and Internacional Symposium on Tectonics of the
936 SBG, Lençóis, pp. 80-90.
- 937 Nogueira, J.F., 2004. Estrutura, geocronologia e alojamento dos batólitos de Quixadá, Quixeramobim e
938 Senador Pompeu - Ceará Central (Doctoral dissertation). Universidade Estadual Paulista, Rio Claro.
- 939 Ortega, J.A., Gómez-Heras, M., Perez-López, R., Wohl, E., 2014. Multiscale structural and lithologic
940 controls in the development of stream potholes on granite bedrock rivers. *Geomorphology* 204, 588
941 – 598. <https://doi.org/10.1016/j.geomorph.2013.09.005>.
- 942 Pedersen, G.B. M., Head III, J.W., Wilson, L., 2010. Formation, erosion and exposure of Early
943 Amazonian dikes, dike swarms and possible subglacial eruptions in the Elysium Rise/Utopia Basin
944 Region, Mars. *Earth and Planetary Science Letters* 294, 424-439.
945 <https://doi.org/10.1016/j.epsl.2009.08.010>.
- 946 Pedraza, J., Angel Sanz, M., Martín, A., 1989. Formas graníticas de la Pedriza. Agencia de Medio
947 Ambiente, Madrid.
- 948 Peulvast, J-P., Claudino Sales, V., 2004. Stepped surfaces and palaeolandforms in the northern Brazilian
949 «Nordeste»: constraints on models of morphotectonic evolution. *Geomorphology* 62, 89-122.
950 <https://doi.org/10.1016/j.geomorph.2004.02.006>.
- 951 Pinéo, T.R.G.; Palheta, E.S.M.; Costa, F.G.; Vasconcelos, A.M.; Gomes, I.P.; Gomes, F.E.M.G.; Bessa,
952 M D M R.; Lima, A F.; Holanda, J L R.; Freire, D P C., 2020. Mapa Geológico do estado do Ceará.
953 2020. CPRM. <http://rigeo.cprm.gov.br/jspui/handle/doc/20418> (accessed 10 Oct 2020).
- 954 Place, J., Géraud, Y., Diraison, M., Herquel, G., Edel, J. -B., Le Garzic, E., Walter, B., 2016. Structural
955 control of weathering processes within exhumed granitoids: Compartmentalisation of geophysical
956 properties by faults and fractures. *Journal of Structural Geology* 84, 102-119.
957 <https://doi.org/10.1016/j.jsg.2015.11.011>.
- 958 Pollard, D.D., Townsend, M.R., 2018. Fluid-filled fractures in Earth's lithosphere: Gravitational loading,
959 interpenetration, and stable height of dikes and veins. *Journal of Structural Geology* 109, 38-54.
960 <https://doi.org/10.1016/j.jsg.2017.11.007>.
- 961 Pye, K., 1986. Mineral and textural controls on the weathering of granitoid rocks. *Catena* 13, 47-57.
- 962 Pye, K., Goudie, A.S., Watson, A., 1986. Petrological influence on differential weathering and inselberg
963 development in the Kora area of Central Kenya. *Earth Surface Processes and Landforms* 11, 41-52.
- 964 Römer, W., 2007. Differential weathering and erosion in an inselberg landscape in southern Zimbabwe:
965 A morphometric study and some notes on factors influencing the long-term development of
966 inselbergs. *Geomorphology* 86, 349-368. <https://doi.org/10.1016/j.geomorph.2006.09.008>.
- 967 Römer, W., 2005. The distribution of inselbergs and their relationship to geomorphological, structural
968 and lithological controls in Southern Zimbabwe. *Geomorphology* 72, 156-176.
969 <https://doi.org/10.1016/j.geomorph.2005.05.008>.
- 970 Roques, C. Bour, O., Aquilina, L., Dewandel, B., Leray, S., Scroetter, J.M., Longueverne, T., Le Borgne,
971 T., Hochereutener, R., Labasque, T., Lavenant, N., Vergnaud-Ayraud, V., Mougin, B., 2014.
972 Hydrological behavior of a deep sub-vertical fault in crystalline basement and relationships with
973 surrounding reservoirs. *Journal of Hydrology* 509, 42-54.
974 <https://doi.org/10.1016/j.jhydrol.2013.11.023>.

- 975 Selby, M.J., 1982. Form and origin of some bornhardts of the Namib Desert. *Zeitschrift für*
 976 *Geomorphologie NF* 26, 1-15.
- 977 Shang, J., 2020. Rupture of veined granite in polyaxial compression: insights from three-dimensional
 978 discrete element method modeling. *Journal of Geophysical Research: Solid Earth* 125, 1-25.
 979 <https://doi.org/10.1029/2019JB019052>.
- 980 Sial, A.N.S., 1986. Granite-types of Northeast Brazil: current knowledge. *Revista Brasileira de*
 981 *Geociências* 16, 54-72.
- 982 Silva, H.F., 1989. Alguns aspectos petrográficos e geoquímicos do Batólito de Quixadá. *Revista*
 983 *brasileira de Geociências* 19, 101-107.
- 984 Stead, D., Wolter, A., 2015. A critical review of rock slope failure mechanisms: The importance of
 985 structural geology. *Journal of Structural Geology* 74, 1-23. <https://doi.org/10.1016/j.jsg.2015.02.002>.
- 986 Thomas, M.F., 1965. Some aspects of the geomorphology of domes and tors in Nigeria. *Zeitschrift für*
 987 *Geomorphologie NF* 9, 63-81.
- 988 Thomas, M.F., 1978. The study of inselbergs. *Zeitschrift für Geomorphologie NF, Supplement-Band*
 989 31, 1-41.
- 990 Torquato, J.R.F. (Coord), Almeida, A.R., Sidrim, A.C.G., Maranhão, C.M.L., Parente, C.V., Torquato,
 991 J.R.F., Neto, A.N., Filho, J.F.A., Souza, J.V., Souza, M.J.N., Arthaud, M.H., 1989. Granitóides do
 992 Ceará: Região de Quixadá e Solonópole [special issue]. *Revista de Geologia* 2, 1-173.
- 993 Turichshev, A., Hadjigeorgiou, J., 2017. Quantifying the effects of vein mineralogy, thickness, and
 994 orientation on the strength of intact veined rock. *Engineering Geology* 226, 199-207.
 995 <https://doi.org/10.1016/j.enggeo.2017.06.009>.
- 996 Twidale, C.R., 1971. *Structural Landforms*. Australian National University Press, Canberra.
- 997 Twidale, C.R., 1981. Granitic inselbergs: domed, block-strewn and castellated. *Geographical Journal*,
 998 147, 54-71.
- 999 Twidale, C.R., 1982. *Granite Landforms*. Elsevier, Amsterdam.
- 1000 Twidale, C.R., 1998. Granitic bornhardts: their morphology, characteristics and origins. *Geological*
 1001 *Society of Malaysia* 42, 237–255.
- 1002 Twidale, C.R., 2002. The two-stage concept of landform and landscape development
 1003 involving etching: origin, development and implications of an idea. *Earth Science Reviews* 57, 37-74.
- 1004 Twidale, C.R., Bourne, J.A., 1975. Episodic exposure of inselbergs. *Geological Society of America*
 1005 *Bulletin* 86, 1473-1481.
- 1006 Twidale, C.R., Campbell, E.M., 1993. Fractures: a double edged sword. A note on fracture density and
 1007 its importance. *Zeitschrift für Geomorphologie NF* 37, 459-475.
- 1008 Twidale, C.R., Vidal-Romaní, J.R., 1994. On the multistage development of etch forms.
 1009 *Geomorphology* 11, 107–124.
- 1010 Twidale, C.R., Vidal-Romaní, J.R., 2005. *Landforms and Geology of Granite Terrains*. Taylor &
 1011 Francis, London.
- 1012 Twidale, C.R., Vidal-Romaní, J.R., 2020. Are corestones due to weathering and/or tectonism? Problems
 1013 and suggestions. *Cadernos do Laboratorio Xeolóxico de Laxe* 42, 29-52.
- 1014 Varajão, C.A.C., de Alkmin, F.F., 2015. Pancas: The kingdom of bornhardts. In: Vieira, B.C., Salgado,
 1015 A.A.R., Santos, L.J.C. (Eds.), *Landscapes and Landforms of Brazil*. Springer, Dordrecht, pp. 381–
 1016 388. DOI 10.1007/978-94-017-8023-0_35.
- 1017 Vauchez, A., Neves, S.P, Caby, R., Corsini, M., Egydio-Silva, M., Arthaud, M., Amaro, V., 1995. The
 1018 Borborema shear zone system, NE Brazil. *Journal of South American Earth Sciences* 8, 247-266.

Souza et al 2023 – Geomorphology [j.geomorph.2023.108865](https://doi.org/10.1016/j.geomorph.2023.108865)

- 1019 Vick, L.M.; Böhme, M.; Rouyet, L.; Bergh, S.G.; Corner, G.D.; Lauknes, T.R. 2020. Structurally
1020 controlled rock slope deformation in northern Norway. *Landslides*, 17, 1745-1776. DOI:
1021 10.1007/s10346-020-01421-7.
- 1022 Vidal-Romani, J.R., 2008. Forms and structural fabric in granite rocks. *Cadernos do Laboratorio*
1023 *Xeolóxico de Laxe* 33, 175–198.
- 1024 Vollgger, S.A., Cruden, A.R., 2016. Mapping folds and fractures in basement and cover rocks using
1025 UAV photogrammetry, Cape Liptrap and Cape Paterson, Victoria, Australia. *Journal of Structural*
1026 *Geology* 85, 168–187. <https://doi.org/10.1016/j.jsg.2016.02.012>.
- 1027 Williams, R.B.G., Robinson, D.A., 1983. The effect of surface texture on the determination of the
1028 surface hardness of rock using the Schmidt Hammer. *Earth Surface Processes and Landforms* 8, 289-
1029 292.